Mathematical and Computer Modelling 52 (2010) 1403–1422

Contents lists available at ScienceDirect

Mathematical and Computer Modelling

journal homepage: www.elsevier.com/locate/mcm

A model for the evolution of concrete deterioration due to reinforcement corrosion

Hossein M. Shodja *, Keivan Kiani, Alireza Hashemian

Department of Civil Engineering, Center of Excellence in Structures and Earthquake Engineering, P.O. Box 11155-9313, Sharif University of Technology, Tehran, Iran

ARTICLE INFO

Article history:
Received 23 November 2009
Received in revised form 22 May 2010
Accepted 25 May 2010

Keywords:
Reinforcement corrosion
Reinforced concrete structures
Microcracking
Mathematical modeling
Analytical solution
Gradient reproducing kernel particle method (GRKPM)

ABSTRACT

One of the most crucial factors affecting the service life of reinforced concrete (RC) structures attacked by aggressive ions is reinforcement corrosion. As the steel corrosion progresses, crack propagation in concrete medium endangers the serviceability and the strength of RC structural members. In this study, a nonlinear mathematical model for determining the displacement and stress fields in RC structures subjected to reinforcement corrosion is introduced. For corrosion products, a nonlinear stress–strain relation which has been previously confirmed by experimental data is incorporated in the present analysis. In formulation of the governing equations for steel–rust–concrete composite, the rational behavior of corrosion products and penetration of rust into the microcracks are considered. An analytical approach as well as an innovative meshless method, gradient reproducing kernel particle method (GRKPM), are employed for solving the nonlinear boundary value problem. A reasonably good agreement between the results of the two methods is achieved. The performance of the proposed model is then investigated through various comparisons of predicted values with experimentally observed data, and again good agreement is obtained. Moreover, the effects of the crucial parameters associated with the mechanical behavior of rust and concrete on time to cover cracking and some measures of deterioration are studied for different values of rust penetration into the microcracks.

1. Introduction

Reinforcement corrosion due to its role in causing severe damage to reinforced concrete (RC) structures has been increasingly paid attention to by the scientific communities of various disciplines during the past three decades. It is believed that reduction in the pH level in electrolyte, which is present in the concrete pores near the rebar, occurs as the aggressive ion concentration (such as chloride and sulfate ions) reaches the threshold value. This chemical process is followed by removal of the passive film over the rebar [1–3]. As a result, the anode and cathode will be configured and the corrosion electrochemical reactions will start. The corrosion products occupy more volume than the original steel rebar and thus the corrosion processes accompany expansive pressure on the concrete's inner surface. The increasing trend of rust production to a threshold value results in the initiation of microcracks around the reinforcement. Loss of load transfer between the concrete medium and the rebar as well as the decrease of the concrete's strength are a manifestation of the increase in corrosion products at the rebar–concrete interface and crack growth within the concrete. As the corrosion reactions continue, these two factors become serious threats to the service life of such RC structures. Hence, if one could properly model rust production and concrete damage mechanisms due to rebar corrosion, it would be of great value in realizing failure prevention measures and more accurate service life predictions of the structures.

* Corresponding author. Tel.: +98 21 6616 4209; fax: +98 21 6607 2555.
E-mail addresses: shodja@sharif.edu (H.M. Shodja), k_kiani@civil.sharif.edu (K. Kiani), al.hash@gmail.com (A. Hashemian).

0895-7177/$ – see front matter © 2010 Elsevier Ltd. All rights reserved.
doi:10.1016/j.mcm.2010.05.023

Bazant [1] presented an analytical model for predicting the time to cover cracking. His theory accounts for the reinforcement diameter, cover thickness, the tensile strength of concrete, the corrosion rate and the corrosion products' density. Dagher and Kulendran [4] considered the formation of smeared cracks caused by the exertion of uniform pressure from the corrosion products at the reinforcement concrete's interface. It was found that a radial expansion of 0.008 mm is sufficient to cause degradation in concrete bridge decks. Molina et al. [5] also used a smeared crack model for the finite element analysis of cover cracking due to reinforcement corrosion. The corrosion of a steel element is modeled by presuming a linear variation of the material properties from those of steel to those of rust. Due to lack of information, they assumed that the mechanical properties of rust nearly resembles that of water which is one of the main constituents of rust. Their analysis was based on the experiments of Andrade et al. [6] where the thickness of the concrete cover was 1.25 and 1.9 times the reinforcement diameter. They found that a corrosion penetration of 0.02 mm was sufficient to initiate a surface crack in the specimens. Noghabai [7] adopted an analytical model for the splitting capacity of a thick-walled concrete ring subjected to an inner pressure based on nonlinear fracture mechanics. Based on field and laboratory data, Morinaga [8] suggested an empirical equation for predicting the time to cover cracking without reference to the evolution of the damage zone. His empirical equation accounts for the time to cover cracking as a function of the corrosion rate, concrete cover thickness and reinforcing diameter. A close scrutiny of the literature [9,10] reveals that the cover cracking predicted by Morinaga's model is much shorter than the experimentally observed values. Pantazopoulou and Papoulia [11] developed an analytical model to investigate how corrosion products cause concrete cover cracking which endangers the service life of RC structures. They assumed that the rebar and the corrosion products behave like a rigid material. Moreover, the corrosion production is simply modeled by imposing a radial displacement on the inner surface of concrete. They investigated the effects of cover thickness, material properties of concrete, and the rate of rust accumulation on the time of cover cracking. However, further investigations in this field have revealed that the consideration of the appropriate mechanical behavior of corrosion products strongly affects the predicted results [12]. Lundgren [13], in an effort to study rebar pull-out, presented a reasonable way to model the effect of corrosion on the bond between the corroded reinforcement and concrete. Lundgren employed finite element analysis and assumed that rust behaves like granular materials, in accordance with the experimental tests of Andrade et al. [6], Al-Sulaimani et al. [14], Cabrera and Ghoddoussi [15], and Ghandehari et al. [16]. In another work, Lundgren [17] used the previously developed model of rust ([13]) together with a bond mechanism model to explore the effect of uniform and localized corrosion on RC beams with corroded reinforcements. Lundgren pointed out that the model could predict the decrease of the bond when splitting of the concrete occurs. It was emphasized that axisymmetric analysis appears to be a satisfactory level of modeling when a study of concrete cover cracking due to uniform corrosion is of concern. However, three dimensional models should be used if localized corrosion is to be studied. The Young's modulus of iron oxides was measured by Ouglova et al. [18] from both ultrasonic measurements and mechanical tests. The tests were performed on dried iron oxides which were in a powder state. The chemical structure of the laboratory grown oxides were similar to those obtained from 40-year old corroded RC structures. The results showed that iron oxides exhibit a nonlinear behavior with notable plastic strain similar to the powder materials. These results confirm those obtained by Lundgren [13,17]. Moreover, the elastic modulus of iron oxides increases with the oxide's volume fraction and drying time of the iron oxides. Recently, Bhargava et al. [10,19,20] presented a mathematical model to predict the time to concrete cover cracking and weight loss of reinforcing bars. However, they assumed that the mechanical properties of corrosion products are the same as those of steel, though reasonably good agreement was obtained between experimental results and the analytical predictions. They showed that tensile strength, initial tangent modulus of concrete, annual mean corrosion rate, and modulus of elasticity of the reinforcement and corrosion significantly influence the predicted time to cover cracking.

In this paper a nonlinear mathematical model is formulated to determine the displacement and stress field in RC structures due to rebar corrosion. The reasonable modeling of the mechanical behavior of rust and the penetration of the corrosion products into the microcracks leads to the nonlinearity of the governing boundary value problem (BVP) of the steel–rust–concrete composite. For this problem, both analytical and numerical solutions are provided. It is proposed to employ an innovative meshless scheme in which the gradient term is incorporated into the reproducing equation of the reproducing kernel particle method (RKPM) [21]. This new approach, presented by Shodja and Hashemian, is called the gradient RKPM (GRKPM) because of the added gradient term [22]. Later, Hashemian and Shodja [23] extended the GRKPM from one to three-dimensional Euclidean space. Application of the GRKPM to the problems of beam–columns and plates shows remarkable results [22,23]. Furthermore, the high performance and accurate resolution of GRKPM when dealing with the Burgers and Buckley–Leverett equations exhibiting evolutionary high gradients and shocks are well established [24,25].

In meshless techniques, the domain of interest is discretized via particles. Therefore, there is no mesh distortion when the medium experiences large deformations. Furthermore, any refinement is possible at a small cost only by inserting additional particles into the desired regions. This remarkable property of meshless methods is particularly attractive for analyzing static and dynamic crack problems as well as problems whose solutions are characterized by steep gradient profiles [26–29]. More detailed surveying of meshless methods has been given in [30]. It should be noted that to overcome the drawback of the finite element method (FEM) in the simulations where mesh distortion occurs, Liu et al. [31] proposed the smoothed finite element method (SFEM) as an alternative technique. They have pointed out that, SFEM generally achieves more accurate results and a higher convergence rate without increasing the computational effort. The convergence and accuracy of SFEM have also been investigated in some detail by Nguyen-Xuan et al. [32]. They concluded that SFEM attains a higher accuracy and convergence rate than the conventional FEM, particularly for incompressible linear elasticity problems.

In the present work, the performance of GRKPM is investigated through various comparisons of the GRKPM solutions with those of the analytical results and experimental data. Moreover, the effects of the parameters associated with the mechanical behavior of rust and concrete, on the variation of crucial parameters of the embedded rebar under corrosion are explored in some detail for various values of rust penetration into microcracks.

2. Mathematical model of rust production

Corrosion of reinforcement can damage poorly designed RC structures. When rebar corrodes, the oxidation products (rust) expand. The corrosion products take up more volume than the virgin steel rebar and therefore, are inclined to deteriorate the concrete by producing microcracks nearby the rebar. Up to the oxidation level, experimental evidence shows that the corrosion products occupy a space as much as six times the volume of the consumed steel. For example, the volume of corrosion products such as FeO, Fe_3O_4, Fe_2O_3, $Fe(OH)_2$, $Fe(OH)_3$ and $Fe(OH)_3.3H_2O$ with respect to the volume of original steel (r_v), are equal to 1.7, 2.0, 2.1, 3.6, 4.0 and 6.15, respectively. Since the molar masses of H_2, O_2 and Fe, in order are 2, 32 and 55.85 grams, the mass of the iron compared to the molecular masses of the above corrosion products (r_m) is equal to 0.777, 0.241, 0.350, 0.622, 0.523 and 0.347, respectively. The production of rust may follow a linear or parabolic law depending on the rust properties [33]. For a metal that does/does not form a protective oxide film, the rate of the corrosion process will be retarded by diffusing of the corrodant ($y^2 = kt$)/constant ($y = kt$) through the film where k, y and t are the corrosion parameter, the film thickness and corrosion time, respectively [33]. It was shown that as the rust layer growth thickens, the ionic diffusion distance increases and the rate of rust production decreases because the diffusion is inversely proportional to the oxide thickness, thereby the rate of corrosion production can be written as follows

$$\frac{\mathrm{d}M_r}{\mathrm{d}t} = \frac{k_p}{M_r}, \tag{1}$$

where M_r is the mass of rust products per unit length of anode in kilograms per meter, t is the corrosion time in seconds and k_p is the rate of rust production which is a function of the corrosion current. By fitting Eq. (1) to the data published by Liu and Weyers [9] and assuming a linear relationship between k_p and corrosion current (I_{corr}), it follows that $k_p = 3.390 \times 10^{-10}\pi D_{st} i_{corr}$, where i_{corr} is the corrosion current density defined as $i_{corr} = \frac{I_{corr}}{\pi D_{st}}$ in amperes per square meters, and D_{st} is the steel diameter in meters. Therefore, if one knows the corrosion current density at each time, the volumes of produced rust and consumed steel can be determined from

$$\begin{aligned} V_r(t) &= \frac{\alpha}{\rho^{st}} \left(\int_0^t 6.78 \times 10^{-10} \pi D_{st} i_{corr} \, \mathrm{d}t \right)^{\frac{1}{2}}, \\ V_s(t) &= \frac{r_m}{\rho^{st}} \left(\int_0^t 6.78 \times 10^{-10} \pi D_{st} i_{corr} \, \mathrm{d}t \right)^{\frac{1}{2}}, \end{aligned} \tag{2}$$

in which ρ^{st} is the steel density in kilograms per cubic meter, α is the ratio of the steel's density to corrosion products' density, $V_r(t)$ and $V_s(t)$ are the produced volume of rust and consumed volume of steel at time t (from beginning of rebar corrosion) in cubic meters per unit length of anode length, correspondingly.

3. Basic assumptions and model definition

The proposed theory accounts not only for the time evolution of pressure buildup due to progressive rusting of the steel reinforcement, but also it incorporates an accurate model descriptive of the behavior of corrosion products. In this, the pressure can be relieved as some volume of the corrosion products move into the generated cracks. To this end, consider a RC member with the cross section as depicted in Fig. 1(a) in which its longitudinal reinforcements are under uniform corrosion. For convenience in analyzing the effects of the reinforcement's corrosion, it is assumed that the only applied load on the member is due to the rebar's corrosion. Moreover, the corrosion of the rebar is a microcell type such that the corrosion current density is uniform on the surface of the rebar along the sizable length of the reinforcement. To determine the displacement and stress fields in the RC media due to rebar corrosion, the problem is modeled as shown in Fig. 1(b), wherein the rebar with an initial radius R_{st} is embedded in concrete with a cover thickness C. Assume the influence domain of the rebar corroding in the concrete medium to be an axisymmetric thick-walled cylinder with internal and external radii of R_r and R_{con}, respectively, in which R_r is the radius of the rust front and $R_{con} = R_{st} + C$. From further numerical scrutinies it is realized that before crack initiation, for $C/R_{st} \geq 8$, the displacement and stress fields due to uniform reinforcement corrosion pertinent to the problem shown in Fig. 1(b) are within reasonable agreement with the corresponding results associated with the axisymmetric problem shown in Fig. 1(c). Due to uniform corrosion of the rebar's surface, the rebar's radius is reduced to R_{cb}, and a thin rust layer with a thickness equal to t_r surrounds the corroded rebar when it is assumed that the corrosion products expand freely (see Fig. 1(c)), then the radius of the rust front is $R_r = R_{cb} + t_r$. As the rebar corrosion reactions maintain, the built up pressure of corrosion products on the inner surface of concrete cylinder increases gradually until the hoop stress of the concrete at the rust–concrete interface becomes greater than the tensile strength of concrete, resulting in a radial microcracks configuration. Smeared cracking is assumed, thereby the displacement and stress fields formulations

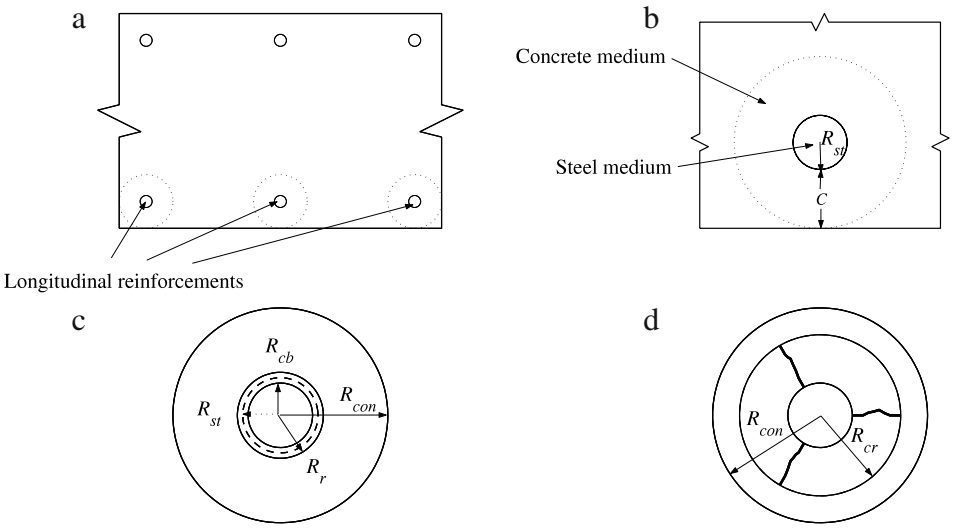

Fig. 1. (a) Cross view of a RC member: longitudinal reinforcements subjected to microcell corrosion, (b) A longitudinal reinforcement with radius R_{st} embedded in concrete with cover thickness C, (c) Geometry of under study steel–rust–concrete composite material (a thick-walled cylinder model), (d) Crack propagation in concrete cover due to rebar corrosion.

are expressed in terms of average displacements and stresses. The smeared crack model has been successfully employed by other researchers [10,19,20,11] to predict the time to cover cracking and the crack width openings of the RC members subjected to the reinforcement corrosion. Axisymmetric loading entails the radial microcracks propagating in all directions with effective radii R_{cr}, called the crack front radii. Therefore, the problem under study is a steel–rust–concrete composite medium as shown in Fig. 1(c). In the remainder of this section, the derivation of the boundary conditions of the mechanical problem is explained in some detail.

If the consumed volume of steel per unit length of anode V_s is determined from rebar weight loss tests or estimated from Eq. (2), then

$$R_{cb} = \sqrt{R_{st}^2 - \frac{V_s}{\pi}}, \tag{3}$$

and if one supposes that the total amount of corrosion products contribute to the pressure buildup; i.e., no corrosion products penetrate into the microcracks, the corrosion products' thickness (t_r) can be readily expressed as

$$t_r = \sqrt{R_{cb}^2 + \frac{V_r}{\pi}} - R_{cb}. \tag{4}$$

On the other hand, the examination of post-corroded specimens shows that not all of the corrosion products contribute to causing pressure, in fact some corrosion products penetrate into the cracks [11]. It should be noted that some of these cracks may have been created due to the internal pressure stemming from corrosion products at the earlier stages. Assuming the smeared crack approach for crack propagation, integration exceedance of the average hoop tensile strain to the cracking strain (ϵ_{cr}) over the ring pyramid, represents a sum of crack width openings. Therefore, the total crack width openings at the interface of rust and concrete can be estimated from the following

$$CWO = \int_0^{2\pi R_r} (\epsilon_\theta - \epsilon_{cr}) \mathrm{d}s = 2\pi \left[u^{con}(R_r) - R_r \epsilon_{cr}\right], \tag{5}$$

where the superscript '*con*' stands for the concrete medium and u is the radial component of displacement field. Before the crack front reaches the concrete outer surface, one may consider this a reasonable assumption ($t_r \ll R_r$). Therefore, with a good approximation

$$CWO = 2\pi \left[u^{con}(R_r) - R_{st} \epsilon_{cr}\right], \tag{6}$$

the total volume of the vacant spaces of microcracks is approximated as $V_{cr} = \frac{1}{2} CWO\,(R_{cr} - R_{st})$. If one supposes that β times of V_{cr} is occupied by corrosion products, then V_r can be written as

$$V_r = \pi (R_r^2 - R_{cb}^2) + \beta\pi \left[u^{con}(R_r) - R_{st} \epsilon_{cr}\right] (R_{cr} - R_{st}). \tag{7}$$

Employing $R_r = R_{cb} + t_r$ and using Eqs. (3) and (7), leads to

$$t_r = -\sqrt{R_{st}^2 - \frac{V_s}{\pi}} + \sqrt{R_{st}^2 + \frac{1}{\pi}(V_r - V_s) - \beta[u^{con}(R_r) - R_{st}\epsilon_{cr}](R_{cr} - R_{st})}, \tag{8}$$

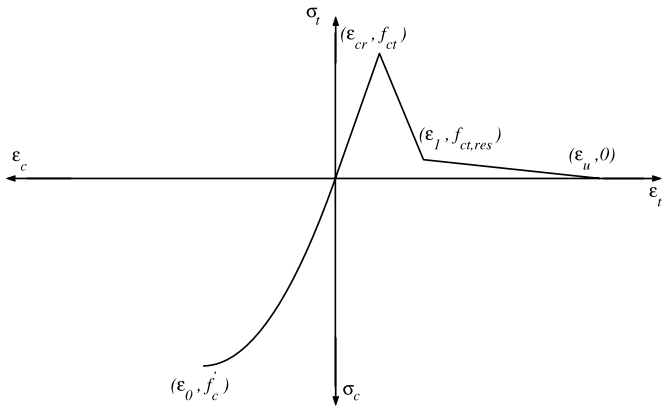

Fig. 2. Mechanical behavior of concrete in uniaxial tension and compression.

where the values of V_r and V_s could be available from laboratory experiments at each time, or estimated from Eq. (2). Most researchers have not considered the appropriate mechanical behavior of rust in their corrosion cracking models. For example, Molina et al. [5] supposed that the mechanical behavior of rust is close to that of water in the liquid state, which is one of the main components of rust. Moreover, they modeled rust as linear elastic material with a Poisson's ratio of 0.5 and a bulk modulus of 2 GPa. They have emphasized that for a more accurate determination of the stress field, incorporation of the realistic behavior of rust is necessary. In the model of corrosion cover cracking proposed by Pantazopoulou and Papoulia [11], it is assumed that rust and steel are rigid. Recently, Bhargava et al. [10,19] assumed that rust and steel exhibit identical linear elastic behavior. Further investigation of Lundgren [13,17] based on the experimental data of other researchers showed that rust behaves like granular materials; its stiffness increases with the stress level. Peter-Lazer and Gerard [34] considered rust material as a cohesionless assemblage of incompressible crystals. Lundgren [13] proposed the power law stress–strain relation for the mechanical behavior of rust under compressive stress. Recently, the experimental results of Ouglova et al. [18] confirm the observations of Lundgren [13] for the behavior of the iron oxide:

$$\sigma_{corr} = K_{corr}(\epsilon_{corr})^{n_{corr}}, \tag{9}$$

where ϵ_{corr} is the compressive strain in the rust layer and σ_{corr} is the corresponding radial compressive stress. Lundgren [13] extracted K_{corr} and n_{corr} from the experiments of other researchers [6,14–16]. This rust model together with a developed bond mechanism model were used in finite element analyses of corrosion cracking problem and pull-out problem with corroded reinforcement, and reported reasonably good agreement with the experimental results of Andrade et al. [6] and Ghandehari et al. [16]. It can readily be shown that the creation of rust between steel and concrete causes a displacement discontinuity. This phenomenon gives rise to the following boundary condition

$$\begin{aligned} &u^{con}(R_r) - u^{st}(R_{cb}) = \delta, \\ &\delta = t_r(1 + \epsilon_{corr}) + R_{cb} - R_{st}, \end{aligned} \tag{10}$$

where t_r, ϵ_{corr}, and R_{cb} are obtained from Eqs. (8) and (9), and (3), respectively. The nonlinear expression of the parameter t_r in terms of u^{con} (see Eq. (8)), and the nonlinear relation between ϵ_{corr} and σ_{corr} lead to a nonlinear BVP. By assuming $t_r \ll R_{st}$, the variation of the radial stress along the rust's thickness is negligible. Hence, the radial stresses at the steel–rust and rust–concrete interfaces are equal

$$\sigma_r^{st}(R_{cb}) \approx \sigma_r^{con}(R_r). \tag{11}$$

In the following sections, the governing equations of steel–rust-cracked concrete composite material will be analyzed by employing both analytical method and the innovative meshless scheme called GRKPM.

4. The governing equations and the analytical solution of the problem

The following assumptions are considered in the proposed cover cracking model due to reinforcement corrosion: (1) The rebar corrosion is a microcell type in which corrosion processes take place similarly over a sizeable length of rebar. Therefore, the problem can be described in 2D; (2) The thickness of the corrosion layer on the rebar's circumference is assumed to be uniform. With this assumption the problem is reduced to an axisymmetric case, which can be treated as a 1D problem; (3) The mechanical behavior of steel, rust and concrete are considered to be linear isotropic, power-law material (see Eq. (9)), and nonlinear anisotropic (see Fig. 2), respectively; (4) The mechanical properties of the concrete are age independent during the rebar's corrosion; (5) The corrosion rate is known at each time of the rebar's corrosion; (6) The amount of corrosion products which penetrate into the microcracks, is known in advanced throughout the corrosion processes.

Considering the first and second assumptions, the governing equilibrium equation of the steel–rust–concrete composite is expressed in the form

$$\sigma_r + r\frac{\mathrm{d}\sigma_r}{\mathrm{d}r} - \sigma_\theta = 0, \tag{12}$$

the elastic strain–displacement relation is

$$\epsilon_r = \frac{\mathrm{d}u}{\mathrm{d}r}, \qquad \epsilon_\theta = \frac{u}{r}, \tag{13}$$

by using the first and second assumptions, the stress–strain relations are derived as

$$\begin{aligned} \sigma_r &= D_{rr}\epsilon_r + D_{r\theta}\epsilon_\theta, \\ \sigma_\theta &= D_{\theta r}\epsilon_r + D_{\theta\theta}\epsilon_\theta, \end{aligned} \tag{14}$$

where the parameters D_{rr}, $D_{r\theta}$, $D_{\theta r}$ and $D_{\theta\theta}$ are as follows for the plane stress case

$$\begin{aligned} D_{rr} &= \frac{E_r}{1-\nu_{r\theta}\nu_{\theta r}}, \qquad D_{r\theta} = \frac{\nu_{r\theta}E_\theta}{1-\nu_{r\theta}\nu_{\theta r}}, \\ D_{\theta r} &= \frac{\nu_{\theta r}E_r}{1-\nu_{r\theta}\nu_{\theta r}}, \qquad D_{\theta\theta} = \frac{E_\theta}{1-\nu_{r\theta}\nu_{\theta r}}, \end{aligned} \tag{15}$$

and for the plane strain case

$$\begin{aligned} D_{rr} &= \frac{E_r\,(1-\nu_{\theta z}\nu_{z\theta})}{\Delta}, \qquad D_{r\theta} = \frac{E_\theta\,(\nu_{r\theta}+\nu_{rz}\nu_{z\theta})}{\Delta}, \\ D_{\theta r} &= \frac{E_r\,(\nu_{\theta r}+\nu_{\theta z}\nu_{zr})}{\Delta}, \qquad D_{\theta\theta} = \frac{E_\theta\,(1-\nu_{rz}\nu_{zr})}{\Delta}, \\ \Delta &= 1-\nu_{\theta z}\nu_{z\theta}-\nu_{rz}\nu_{zr}-\nu_{r\theta}\nu_{\theta r}-\nu_{r\theta}\nu_{\theta z}\nu_{zr}-\nu_{rz}\nu_{z\theta}\nu_{\theta r}, \end{aligned} \tag{16}$$

in which E_r and E_θ denote the modulus of elasticity in the radial and hoop directions, respectively; and $\nu_{r\theta}$, $\nu_{\theta r}$, ν_{rz}, ν_{zr}, $\nu_{\theta z}$, $\nu_{z\theta}$ are the Poisson's ratios. The symmetry of the anisotropic stiffness matrix reads, $D_{r\theta} = D_{\theta r}$. Therefore, by substituting the strain components in terms of radial displacement in Eq. (14), and substituting the resulting stress components in Eq. (12), the governing equation in terms of radial displacement takes the following form

$$r^2\frac{\mathrm{d}^2u}{\mathrm{d}r^2} + r\frac{\mathrm{d}u}{\mathrm{d}r} - \kappa^2 u = 0, \tag{17}$$

where $\kappa^2 = D_{\theta\theta}/D_{rr}$. Since the problem is assumed to be axisymmetric, the hoop and the radial stresses are the tensile and compressive principal stresses, respectively. Smeared cracks are assumed to configure in the radial directions as the hoop stress exceeds the tensile capacity of concrete. The assumed stress–strain relationship for the principal tensile and compressive stresses is presented in Fig. 2. Under compression, the behavior of concrete follows a Hognestad-type parabola with the initial modulus of elasticity E_0 which is set to be $15\,100\sqrt{f_c'}$ for normal concrete [35] where f_c' is the uniaxial compressive strength, and the radial elastic modulus (E_r) is defined by the secant slope of the compression stress–strain curve. In the principal tensile direction, the relationship between the tensile stress (σ_θ) and tensile strain (ϵ_θ) in concrete is assumed to be linear with a slope equal to E_0 before cracking. Cracking in concrete is modeled as a softening process that begins with the exceedance of the hoop strain from the tensile strain capacity of concrete ($\epsilon_\theta > \epsilon_{cr} = f_{ct}/E_0$). The value of f_{ct} varies between $1.6\sqrt{f_c'}$ and $1.85\sqrt{f_c'}$ [35] and is taken here as $1.725\sqrt{f_c'}$ (where the unit of f_c' is kg/cm^2). The softening behavior of concrete in tension is assumed to be bilinear; see Fig. 2, in which the tensile strains of ϵ_1 and ϵ_u correspond to the tensile stresses of $0.15f_c'$ (i.e., residual tensile strength) and 0, determined based on the maximum aggregate size of the concrete mix and fracture energy of the concrete [36,37].

It is worth mentioning that crack propagation within a concrete medium changes the homogeneous medium into a nonhomogeneous one (cracked concrete). This effect is considered in the proposed analytical model by the parameter κ which is a function of medium's material properties. Dependency of κ to the parameter r in the cracked concrete medium results in the complexity of finding a closed form solution for Eq. (17). To overcome this difficulty, one can divide the concrete medium into N layers such that the parameter κ has a constant value within each layer with a good approximation (as shown in Fig. 3). Therefore, the solution of Eq. (17) is

$$u = Ar^{\kappa} + Br^{-\kappa}, \tag{18}$$

by substituting Eq. (18) into Eq. (13), the strain components are derived as

$$\begin{aligned} \epsilon_r &= A\left(\kappa r^{\kappa-1}\right) - B\left(\kappa r^{-\kappa-1}\right), \\ \epsilon_\theta &= Ar^{\kappa-1} + Br^{-\kappa-1}, \end{aligned} \tag{19}$$

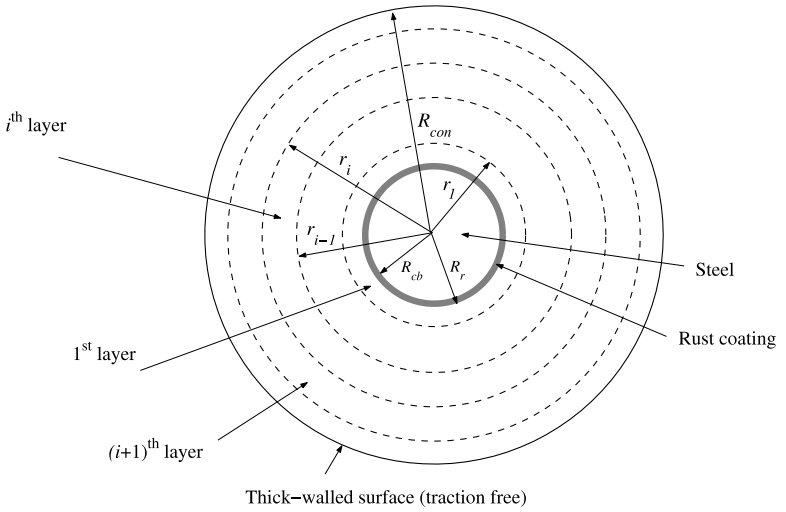

Fig. 3. Topography of steel–rust–concrete composite utilized for solving the BVP via an analytical approach.

and by substituting Eq. (19) with Eq. (14), the stress components are expressed as

$$\begin{aligned}\sigma_r &= A\,(D_{r\theta}+\kappa D_{rr})\,r^{\kappa-1}+B\,(D_{r\theta}-\kappa D_{rr})\,r^{-\kappa-1},\\ \sigma_\theta &= A\,(D_{\theta\theta}+\kappa D_{r\theta})\,r^{\kappa-1}+B\,(D_{\theta\theta}-\kappa D_{r\theta})\,r^{-\kappa-1}.\end{aligned} \tag{20}$$

It should be noted that when the generated microcracks cause damage such that $E_\theta = 0$ and subsequently $\kappa = 0$, the only nonzero displacement and stress component take the following form

$$\begin{aligned}u &= A + B\ln(r),\\ \sigma_r &= BD_{rr}r^{-1},\end{aligned} \tag{21}$$

for convenience, the radial displacement, radial and hoop stresses within the ith layer are expressed as

$$\begin{aligned}u_i^{con}(r) &= A_i\mathcal{P}_i(r)+B_i\mathcal{Q}_i(r),\\ \sigma_{r,i}^{con}(r) &= A_i\mathcal{R}_i(r)+B_i\mathcal{S}_i(r),\\ \sigma_{\theta,i}^{con}(r) &= A_i\mathcal{V}_i(r)+B_i\mathcal{W}_i(r),\end{aligned} \tag{22}$$

no sum on i, $i = 1, 2, \ldots, N$. The functions $\mathcal{P}_i$, $\mathcal{Q}_i$, $\mathcal{R}_i$, $\mathcal{S}_i$, $\mathcal{V}_i$ and $\mathcal{W}_i$ are defined as

$$\mathcal{P}_i(r) = \begin{cases} r^{\kappa_i}, & \kappa_i \neq 0\\ 1, & \kappa_i = 0\end{cases}, \qquad \mathcal{Q}_i(r) = \begin{cases} r^{-\kappa_i}, & \kappa_i \neq 0\\ \ln(r), & \kappa_i = 0\end{cases}, \tag{23}$$

$$\begin{aligned}\mathcal{R}_i(r) &= \begin{cases}(D_{r\theta}+\kappa D_{rr})_i\,r^{\kappa_i-1}, & \kappa_i\neq 0\\ 0, & \kappa_i = 0\end{cases},\\ \mathcal{S}_i(r) &= \begin{cases}(D_{r\theta}-\kappa D_{rr})_i\,r^{-\kappa_i-1}, & \kappa_i\neq 0\\ D_{rr}r^{-1}, & \kappa_i = 0\end{cases},\end{aligned} \tag{24}$$

$$\begin{aligned}\mathcal{V}_i(r) &= \begin{cases}(D_{\theta\theta}+\kappa D_{r\theta})_i\,r^{\kappa_i-1}, & \kappa_i\neq 0\\ 0, & \kappa_i = 0\end{cases},\\ \mathcal{W}_i(r) &= \begin{cases}(D_{\theta\theta}-\kappa D_{r\theta})_i\,r^{-\kappa_i-1}, & \kappa_i\neq 0\\ 0, & \kappa_i = 0\end{cases}.\end{aligned} \tag{25}$$

The third assumption for the steel medium reads, $E_r = E_z = E_\theta = E^{st}$, $\nu_{rz} = \nu_{r\theta} = \nu_{\theta z} = \nu^{st}$, and so $\kappa = 1$, in which E^{st} is the elastic modulus of the steel rebar, and ν^{st} is its Poisson's ratio. Therefore, the displacement and stress components in steel take the following form

$$\begin{aligned}u^{st}(r) &= A_0\,r,\\ \sigma_r^{st}(r) &= A_0(D_{rr}^{st}+D_{r\theta}^{st}),\\ \sigma_\theta^{st}(r) &= A_0(D_{rr}^{st}+D_{r\theta}^{st}).\end{aligned} \tag{26}$$

Consequently, the only unknown parameter of the rebar is A_0, and so for analysis of steel–rust–concrete composite, there is a total of $2N + 1$ unknowns which should be determined by imposing the proper boundary conditions. In addition to the

interface conditions (10) and (11), the continuity of the radial component of the displacement and stress fields across the boundary between ith and $(i+1)$th layer requires that

$$u_i^{con}(r_i) = u_{i+1}^{con}(r_i), \qquad \sigma_{r,i}^{con}(r_i) = \sigma_{r,i+1}^{con}(r_i), \quad i = 1, 2, \ldots, N-1 \tag{27}$$

respectively. In the above condition, r_i indicates the radius of the interface between the ith and $(i+1)$th regions, Fig. 3. On the outer surface of the concrete medium

$$\sigma_r^{con}(r_N) = 0. \tag{28}$$

Imposing the conditions (10), (11), (27) and (28)

$$\mathbf{K}\mathbf{x} = \mathbf{f}_{corr}, \tag{29}$$

is obtained. Where the elements of the coefficient matrix $\mathbf{K}$ are given in Appendix. In relation (29)

$$\mathbf{x} = [A_0 \quad A_1 \quad B_1 \quad \ldots \quad A_i \quad B_i \quad A_{i+1} \quad B_{i+1} \quad \ldots \quad A_N \quad B_N]^T, \tag{30}$$

$$\mathbf{f}_{corr} = [\delta \quad 0 \quad 0 \quad \ldots \quad 0 \quad 0 \quad 0 \quad 0 \quad \ldots \quad 0 \quad 0]^T. \tag{31}$$

It should be noted that the corrosion force ($\mathbf{f}_{corr}$) is a nonlinear vector function of the radial stress component at the rust–concrete interface; see Eq. (10). Therefore, Eq. (29) is a nonlinear equation set, which should be solved by a suitable and effective method at each time step. To solve the system of nonlinear equations, Newton's method is utilized. The residual vector function is therefore defined as

$$\mathbf{R}(\mathbf{x}) = \mathbf{K}\mathbf{x} - \mathbf{f}_{corr}, \tag{32}$$

consider the first two terms in the Taylor expansion series of $\mathbf{R}(\mathbf{x})$ about $\widetilde{\mathbf{x}}$, which is the previous value of $\mathbf{x}$ in the iteration process, in which applying $\mathbf{R}(\mathbf{x}) = \mathbf{0}$ gives

$$\overline{\mathbf{K}}\Delta\mathbf{x} = \bar{\mathbf{f}}, \tag{33}$$

where

$$\overline{\mathbf{K}}_{ij} = \begin{cases} \mathbf{K}_{ij} - \dfrac{t_r}{n_{corr}}\left[\dfrac{D_{rr}^{st} + D_{r\theta}^{st}}{K_{corr}}\right]^{\frac{1}{n_{corr}}} A_0^{\frac{1-n_{corr}}{n_{corr}}} & i = 1,\ j = 1 \\ \mathbf{K}_{ij} + \dfrac{1}{2}\beta\lambda\mathcal{P}_1(R_r) & i = 1,\ j = 2 \\ \mathbf{K}_{ij} + \dfrac{1}{2}\beta\lambda\mathcal{Q}_1(R_r) & i = 1,\ j = 3 \\ \mathbf{K}_{ij} & \text{otherwise} \end{cases}, \tag{34}$$

$$\Delta\mathbf{x} = \mathbf{x} - \widetilde{\mathbf{x}},$$

$$\bar{\mathbf{f}}(\widetilde{\mathbf{x}}) = \mathbf{f}_{corr}(\widetilde{\mathbf{x}}) - \mathbf{K}\widetilde{\mathbf{x}},$$

in which

$$\lambda = \left\{R_{st}^2 + \frac{1}{\pi}(V_r - V_s) - \beta[u^{con}(R_r) - R_{st}\epsilon_{cr}]\right\}^{-\frac{1}{2}} (R_{cr} - R_{st})^{\frac{1}{2}}(1 + \epsilon_{corr}), \tag{35}$$

the unknown parameters of Eq. (33) could be determined by doing iterative operations until getting accurate results at each time step. In this work, the convergence criterion is set to be $\|\Delta\mathbf{x}\|/\|\mathbf{x}\| < 10^{-10}$.

For convenience, the algorithm for the nonlinear analysis of the problem is provided below:

1. Initial conditions of the problem: set $t = 0$, $\epsilon_{corr} = 0$, $R_{cr} = R_{st}$, and $\mathbf{x} = \widetilde{\mathbf{x}} = \mathbf{0}$.
2. Determination of $V_r(t)$ and $V_s(t)$ from Eq. (2) and evaluation of R_{cb} from Eq. (3).
3. Newton's iterations at time t:
   a. evaluation of κ and strain field within the steel and the layers of the damaged concrete media.
   b. compute t_r and δ from Eqs. (8) and (10).
   c. update $\mathbf{K}$ and $\mathbf{f}_{corr}$.
   d. compute $\overline{\mathbf{K}}$ and $\bar{\mathbf{f}}(\widetilde{\mathbf{x}})$ according to Eq. (34).
   e. solve the linear set of equations $\Delta\mathbf{x} = \overline{\mathbf{K}}^{-1}\bar{\mathbf{f}}$.
   f. $\mathbf{x} = \mathbf{x} + \Delta\mathbf{x}$.
   g. check the convergence criterion; if met go to step 4; otherwise, go to step a.
4. $\widetilde{\mathbf{x}} = \mathbf{x}$, $t = t + \Delta t$.
5. The required outputs are produced. If the final time is not reached, go to step 2.

5. The numerical solution via GRKPM

Recent developments in meshless methodologies have provided an alternative powerful tool for visiting various challenging problems exhibiting nonlinearity, large deformations, or high gradients. In contrast to the finite element method (FEM) not only is mesh generation time saved but also the mesh recreation time is eliminated. Moreover, the problem of encountering awkward elements is circumvented. This attractive advantage of the meshless approaches is the reason for turning the attention of many scientists to either its further development or its implications as an alternative approach. Nowadays there are many periodical and annual international events focusing on various aspects of meshless methods. The present boundary value problem (BVP), due to the presence of interfaces and the rust layer whose thickness varies with time, is quite challenging when seeking an accurate numerical solution. To this end, GRKPM is utilized to solve the proposed BVP. GRKPM is advantageous for solving BVPs which are governed by fourth order differential equations [22,23]. For problems for which the solution in some regions is described by steep gradient profiles, GRKPM provides an accurate result [24,25]. Moreover, when the essential boundary conditions involve the first derivative of the field quantity, they can be satisfied exactly by applying a corrected collocation method. This treatment yields a higher convergence rate than RKPM [22,23]. GRKPM involves two, three and four types of shape functions for 1D, 2D and 3D problems, respectively. Therefore, it results in a higher number of degrees of freedom (DOFs) in comparison with those of RKPM for a given distribution of particles. A brief introduction to GRKPM is given in Section 5.1. Subsequently the implication of GRKPM to the present problem is provided in Section 5.2.

5.1. A brief description of GRKPM

The RKPM is a meshfree approach in which the function is reproduced through a linear integral transformation by a modified kernel function [21]. For enhanced accuracy, the present work utilizes GRKPM which is a new class of meshless methods [22–25]. In the first order GRKPM [22], the reproducing function is defined in terms of the function and its first derivative

$$u^R(x) = \sum_{k=0}^{1} \int_{\Omega} \overline{\phi}_a^{[k]}(x; x-y) u^{(k)}(y) \mathrm{d}y, \tag{36}$$

where Ω is the space domain, $u^{(0)}(y) = u(y)$ and $u^{(1)}(y) = \frac{\mathrm{d}u}{\mathrm{d}y}$ are the one dimensional field function and its first derivative, respectively. $\overline{\phi}_a^{[k]}$ is the modified kernel function defined as

$$\overline{\phi}_a^{[k]}(x; x-y) = \left[\sum_{s=0}^{1} b_s^{[k]}(x)(x-y)^s\right] \frac{1}{a}\phi\left(\frac{x-y}{a}\right), \quad k = 0, 1. \tag{37}$$

In Eq. (37), a is a dilation parameter, ϕ is a window function and $b_s^{[k]}$, $s = 0, 1$; $k = 0, 1$ are the unknown moving coefficients which are determined in the integration points of the domain through enforcing the completeness conditions. To this end, consider the Taylor series expansion of a third-order polynomial about point x

$$u(y) = \sum_{\alpha=0}^{3} \frac{(-1)^\alpha}{\alpha!}(x-y)^\alpha u^{(\alpha)}(x), \tag{38}$$

substituting Eqs. (37) and (38) into Eq. (36) yields

$$u^R(x) = \sum_{k=0}^{1}\sum_{\alpha=k}^{3}\sum_{s=0}^{1} \frac{(-1)^{\alpha-k}}{(\alpha-k)!} u^{(\alpha)}(x)\, b_s^{[k]}(x)\, m_{\alpha+s-k}(x), \tag{39}$$

in which $m_k(x)$ is the moment function of kth order associated with the window function ϕ

$$m_k(x) = \int_{\Omega} (x-y)^k \frac{1}{a}\phi\left(\frac{x-y}{a}\right) \mathrm{d}y. \tag{40}$$

The completeness condition reads [22]

$$\mathbf{M}(x)\left[b_0^{[0]}(x)\; b_1^{[0]}(x)\; b_0^{[1]}(x)\; b_1^{[1]}(x)\right]^T = [1\,0\,0\,0]^T, \tag{41}$$

where

$$\mathbf{M}(x) = \begin{bmatrix} m_0(x) & m_1(x) & 0 & 0 \\ m_1(x) & m_2(x) & -m_0(x) & -m_1(x) \\ m_2(x) & m_3(x) & -2m_1(x) & -2m_2(x) \\ m_3(x) & m_4(x) & -3m_2(x) & -3m_3(x) \end{bmatrix}. \tag{42}$$

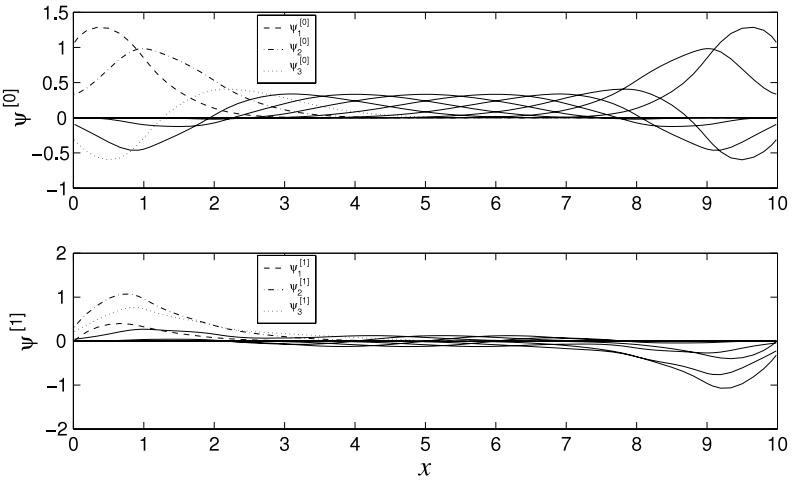

Fig. 4. The GRKPM shape functions of the first (with the superscript [0]) and second kind (with the superscript [1]) for the uniform distribution of particles; the subscripts 1, 2, and 3 represent the shape functions associated with the first, second and third particles, respectively.

$b_s^{[k]}$ can be obtained by solving Eq. (41). To this end, the integral in Eq. (40) should be discretized. Utilizing the trapezoidal method, the reproduced field function, Eq. (36), takes the following discrete form

$$u^R(x) = \sum_{k=0}^{1} \sum_{J=1}^{NP} \psi_J^{[k]} u_J^{(k)}. \tag{43}$$

In the above relation, NP is the number of particles, $u_J^{(k)}$ is the independent degree of freedoms (DOFs) and $\psi_J^{[k]}$ is the shape function of the kth kind associated with the Jth particle

$$\psi_J^{[k]}(x) = \left[\sum_{s=0}^{1} b_s^{[k]}(x)(x - y_J)^s\right] \frac{1}{a}\phi\left(\frac{x - y_J}{a}\right) \Delta y_J. \tag{44}$$

Assume 11 uniformly distributed particles in [0, 10], $a = 1.6$ and a cubic spline for the window function. The GRKPM shape functions of the first and second kind are presented in Fig. 4(a) and (b), respectively. The dash, dash–dot, and dotted lines represent the shape functions associated with the particles located at $x = 0$, 1, and 2, correspondingly. The shape functions' first derivatives are

$$\begin{aligned}\left[\psi_J^{[k]}(x)\right]^{(1)} &= \sum_{s=0}^{1} \left\{ b_s^{[k]}(x) s (x - y_J)^{s-1} + \left[b_s^{[k]}(x)\right]^{(1)} (x - y_J)^s \right\} \frac{1}{a}\phi\left(\frac{x - y_J}{a}\right) \Delta y_J \\ &\quad + \sum_{s=0}^{1} \left[b_s^{[k]}(x)(x - y_J)^s\right] \frac{1}{a}\left[\phi\left(\frac{x - y_J}{a}\right)\right]^{(1)} \Delta y_J,\end{aligned} \tag{45}$$

where $[b_s^{[k]}(x)]^{(1)}$ is determined by differentiating Eq. (41).

5.2. Implication of the GRKPM to the present BVP

Let Γ_{corr} and Γ_{con} denote the steel-concrete interface and the outer boundary of the concrete, respectively; see Fig. 5(a). The conditions on these boundaries are

$$\begin{aligned} u^{con} - u^{st} &= \delta \quad \text{on } \Gamma_{corr}, \\ \sigma_r^{con} &= 0 \quad \text{on } \Gamma_{con}, \end{aligned} \tag{46}$$

where u^{con} and u^{st} refer to the values of the radial displacement inside the concrete and steel zones, respectively. Since the problem is axisymmetric, the field quantities are functions of r only (see Fig. 5(b)), thus the displacement may be expressed as

$$\begin{aligned} u^{st}(r) &= \sum_{J=1}^{NP^{st}} \mathbf{\Psi}_J^{st} \mathbf{u}_J^{st}; \quad \mathbf{\Psi}_J^{st} = [\psi_J^{[0]}, \psi_J^{[1]}]^{st}, \ \mathbf{u}_J^{st} = \{[u_J^{(0)}, u_J^{(1)}]^{st}\}^T, \\ u^{con}(r) &= \sum_{J=1}^{NP^{con}} \mathbf{\Psi}_J^{con} \mathbf{u}_J^{con}; \quad \mathbf{\Psi}_J^{con} = [\psi_J^{[0]}, \psi_J^{[1]}]^{con}, \mathbf{u}_J^{con} = \{[u_J^{(0)}, u_J^{(1)}]^{con}\}^T. \end{aligned} \tag{47}$$

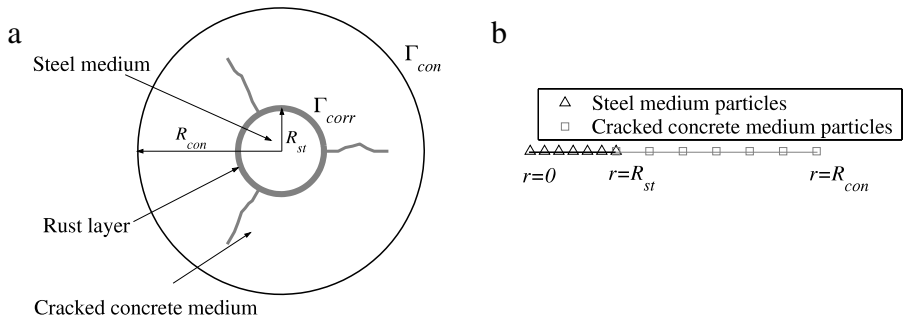

Fig. 5. (a) Schematic of the steel–rust–concrete composite utilized for numerical analysis via GRKPM. (b) Distribution of particles in steel and concrete domains when the penalty method is employed for enforcing the essential boundary conditions.

Using Eqs. (13) and (14)

$$\begin{aligned}\epsilon^{st} &= \sum_{J=1}^{NP^{st}} \left[\Psi^{st}_{J,r}, \frac{\Psi^{st}_J}{r}\right]^T \mathbf{u}^{st}_J = \sum_{J=1}^{NP^{st}} \mathbf{B}^{st}_J \mathbf{u}^{st}_J,\\ \epsilon^{con} &= \sum_{J=1}^{NP^{con}} \left[\Psi^{con}_{J,r}, \frac{\Psi^{con}_J}{r}\right]^T \mathbf{u}^{con}_J = \sum_{J=1}^{NP^{con}} \mathbf{B}^{con}_J \mathbf{u}^{con}_J,\end{aligned} \tag{48}$$

and

$$\begin{aligned}\sigma^{st} &= \mathbf{D}^{st}\epsilon^{st}; \qquad \mathbf{D}^{st} = \begin{bmatrix} D_{rr} & D_{r\theta} \\ D_{r\theta} & D_{rr}\end{bmatrix}^{st},\\ \sigma^{con} &= \mathbf{D}^{con}\epsilon^{con}; \qquad \mathbf{D}^{con} = \begin{bmatrix} D_{rr} & D_{r\theta} \\ D_{r\theta} & D_{\theta\theta}\end{bmatrix}^{con}.\end{aligned} \tag{49}$$

In the present work, the penalty method is employed for enforcing the boundary conditions, Eq. (46). Therefore, the modified total elastic strain energy pertained to the steel–rust–concrete composite is expressed as

$$\pi = \frac{1}{2}\int_{\Omega^{st}\cup\Omega^{con}} \epsilon^T \sigma \,\mathrm{d}\Omega + \frac{1}{2}\int_{\Gamma_{corr}} (u^{con} - u^{st} - \delta)\chi(u^{con} - u^{st} - \delta)\mathrm{d}\Gamma, \tag{50}$$

where χ is the penalty factor which is set equal to $10^5 E^{st}$ in this work. Applying the principle of the minimum total potential energy to Eq. (50) and using Eqs. (47)–(49) yield

$$\mathbf{K}_t\tilde{\mathbf{u}} = \mathbf{f}_{corr},$$

$$[\mathbf{K}_t]_{IJ} = \begin{bmatrix} \int_{\Omega^{st}} \mathbf{B}^{st^T}_I \mathbf{D}^{st}\mathbf{B}^{st}_J \mathrm{d}\Omega & \mathbf{0} \\ \mathbf{0} & \int_{\Omega^{con}} \mathbf{B}^{con^T}_I \mathbf{D}^{con}\mathbf{B}^{con}_J \mathrm{d}\Omega \end{bmatrix} + \begin{bmatrix} \int_{\Gamma_{corr}} \Psi^{st^T}_I \chi \Psi^{st}_J \mathrm{d}\Gamma & -\int_{\Gamma_{corr}} \Psi^{st^T}_I \chi \Psi^{con}_J \mathrm{d}\Gamma \\ -\int_{\Gamma_{corr}} \Psi^{con^T}_I \chi \Psi^{st}_J \mathrm{d}\Gamma & \int_{\Gamma_{corr}} \Psi^{con^T}_I \chi \Psi^{con}_J \mathrm{d}\Gamma \end{bmatrix}, \tag{51}$$

$$\{\mathbf{f}_{corr}\}_I = \begin{Bmatrix} -\int_{\Gamma_{corr}} \Psi^{st^T}_I \chi\delta \,\mathrm{d}\Gamma \\ \int_{\Gamma_{corr}} \Psi^{con^T}_I \chi\delta \,\mathrm{d}\Gamma \end{Bmatrix},$$

$$\tilde{\mathbf{u}} = \left[\mathbf{u}^{st}, \mathbf{u}^{con}\right]^T.$$

It should be noted that the vector function $\mathbf{f}_{corr}$ is nonlinear according to the Eqs. (8) and (9). Employing Newton's method for solving the nonlinear system of Eq. (50), the residual vector function is defined

$$\mathbf{R}(\tilde{\mathbf{u}}) = \mathbf{K}_t\tilde{\mathbf{u}} - \mathbf{f}_{corr}. \tag{52}$$

Considering the first two terms in the Taylor expansion series of $\mathbf{R}(\tilde{\mathbf{u}})$ about $\bar{\mathbf{u}}$, which is the previous value of $\tilde{\mathbf{u}}$ in the iteration process, and applying $\mathbf{R}(\tilde{\mathbf{u}}) = \mathbf{0}$ gives

$$\mathbf{K}(\tilde{\mathbf{u}} - \bar{\mathbf{u}}) = -\mathbf{R}(\bar{\mathbf{u}}), \tag{53}$$

where

$$\mathbf{K} = \mathbf{K}_t - \frac{\chi\, t_r}{n_{corr}K_{corr}}\int_{\Gamma_{corr}} \epsilon_{corr}^{1-n_{corr}}\mathbf{S}\,\mathrm{d}\Gamma + \frac{1}{2}\beta\lambda\chi\int_{\Gamma_{corr}} (1+\epsilon_{corr})\mathbf{M}\mathrm{d}\Gamma, \tag{54}$$

Table 1
Case study data of various RC cylindrical specimens subjected to rebar corrosion used for verification of the results of GRKPM and analytical approach.

Design specimen	D_{st} (cm)	C (cm)	f_c' (MPa)	i_{corr} $\left(\frac{\mu A}{cm^2}\right)$
I	1.6	4.8	30	2500
II	2.0	7.5	35	200
III	1.4	5.0	50	10

Table 2
Comparison the predicted results of GRKPM and those of the analytical approach for various values of β.

Parameter	I		II		III	
	GRKPM [e_{rel}[a]]	Analytical	GRKPM [e_{rel}]	Analytical	GRKPM [e_{rel}]	Analytical
$\beta = 0.00$						
T_{cr} (days)	0.6125 [0.69]	0.6083	26.83 [0.60]	26.67	174 [0.00]	174
W_s (%)	0.831 [0.36]	0.828	1.114 [0.36]	1.110	1.083 [0.00]	1.083
$\frac{\sigma_{r,\max}}{f_t}$	3.222 [0.40]	3.235	3.912 [0.79]	3.943	3.752 [0.58]	3.774
CWO_{cr} (mm)	0.06438 [0.56]	0.06402	0.1036 [0.48]	0.1031	0.06862 [0.48]	0.06829
$\beta = 0.10$						
T_{cr} (days)	0.8250 [1.54]	0.8125	38.33 [0.87]	38.00	244 [0.83]	242
W_s (%)	0.965 [0.84]	0.957	1.331 [0.45]	1.325	1.282 [0.39]	1.277
$\frac{\sigma_{r,\max}}{f_t}$	3.222 [0.40]	3.235	3.912 [0.74]	3.941	3.752 [0.58]	3.774
CWO_{cr} (mm)	0.06396 [0.96]	0.06335	0.1032 [0.58]	0.1026	0.06841 [1.15]	0.06763
$\beta = 0.20$						
T_{cr} (days)	1.071 [2.00]	1.050	52.50 [1.60]	51.67	329 [1.54]	324
W_s (%)	1.099 [1.01]	1.088	1.558 [0.84]	1.545	1.489 [0.81]	1.477
$\frac{\sigma_{r,\max}}{f_t}$	3.222 [0.40]	3.235	3.912 [0.74]	3.941	3.752 [0.58]	3.774
CWO_{cr} (mm)	0.06376 [0.92]	0.06318	0.1033 [0.68]	0.1026	0.06815 [0.81]	0.06760
$\beta = 0.30$						
T_{cr} (days)	1.354 [2.19]	1.325	69.00 [6.15]	65.00	426 [1.91]	418
W_s (%)	1.236 [1.06]	1.223	1.786 [3.06]	1.733	1.694 [0.95]	1.678
$\frac{\sigma_{r,\max}}{f_t}$	3.222 [0.40]	3.235	3.912 [0.74]	3.941	3.752 [0.58]	3.774
CWO_{cr} (mm)	0.06369 [0.87]	0.06314	0.1033 [1.77]	0.1015	0.06805 [0.70]	0.06758

[a] e_{rel} denotes the percentage relative error between the GRKPM results and those of the analytical solution (i.e., $e_{rel} = 100\times|[\,]_{\text{GRKPM}} - [\,]_{\text{Analytical}}|/[\,]_{\text{GRKPM}}$).

in which

$$\mathbf{S}_{IJ} = \begin{bmatrix} \mathbf{0} & -\boldsymbol{\Psi}_I^{stT}(D_{rr}^{con}\boldsymbol{\Psi}_{J,r}^{con} + D_{r\theta}^{con}\boldsymbol{\Psi}_J^{con}/r) \\ \mathbf{0} & \boldsymbol{\Psi}_I^{conT}(D_{rr}^{con}\boldsymbol{\Psi}_{J,r}^{con} + D_{r\theta}^{con}\boldsymbol{\Psi}_J^{con}/r) \end{bmatrix},$$
$$\mathbf{M}_{IJ} = \begin{bmatrix} \mathbf{0} & -\boldsymbol{\Psi}_I^{stT}\boldsymbol{\Psi}_J^{con} \\ \mathbf{0} & \boldsymbol{\Psi}_I^{conT}\boldsymbol{\Psi}_J^{con} \end{bmatrix}. \tag{55}$$

The unknowns in Eq. (53) are determined by applying iterative operations. To this end, the convergence criterion is the same as the one considered in the analytical solution. Moreover, the algorithm for solving of the nonlinear problem is analogous to that mentioned in Section 4.

6. Results and discussion

6.1. Comparison of the analytical and GRKPM results

Consider three different specimens I, II, and III, for which the required data have been outlined in Table 1. The corresponding BVPs are solved under plane stress condition and it is assumed that $\nu_{r\theta} = 0.17$, $\alpha = 2.09$, $r_m = 0.622$, $\rho^{st} = 7850\,(\text{kg/m}^3)$, $E^{st} = 2\times10^{10}\,(\text{kg/m}^2)$, $\nu^{st} = 0.3$. In all of the GRKPM analyses, 11 uniformly distributed particles in each medium, and 4 Gaussian points for each computational cell are considered. The pertinent shape functions are obtained using a linear base function, third order spline window function, and dilation parameter, $a = 4$. Table 2 provides the comparison of the predicted numerical and analytical values from the proposed cover cracking model due to rebar corrosion in terms of T_{cr}, W_s, $\sigma_{r,\max}/f_t$ and CWO_{cr} for various values of β; wherein T_{cr} is the time of surface cracking, W_s is the amount of weight loss of the rebar through the corrosion processes up to the time of concrete surface cracking, $\sigma_{r,\max}/f_t$ is the ratio of the maximum value of radial stress to the tensile strength of concrete, and CWO_{cr} is the crack width openings at the concrete-rust interface when surface cracking occurs. A reasonably good agreement between the GRKPM and analytical solutions is achieved. It is clear that as the value of β increases, the values of the parameters T_{cr} and W_s increase dramatically, but the values of the parameters CWO_{cr} and $\sigma_{r,\max}/f_t$ decrease only slightly.

The estimated values of T_{cr}, W_s, $\sigma_{r,\max}/f_t$ and CWO_{cr} analyzed via the GRKPM and analytical solutions are presented in Table 3 for various values of R_{con}/R_{st} and β, for the specimen designation of III. It is assumed that the value of R_{st} is fixed and the other parameters are as previously mentioned. As the results show, there is a good agreement between the predicted

Table 3
Comparison the predicted results of GRKPM and those of analytical approach for design specimen III for various values of β and R_{con}/R_{st} ratio.

		R_{con}/R_{st}						
		3	4	5	6	7	8	9
$\beta = 0.00$								
Analytical	T_{cr} (days)	10.00	22.50	42.25	71.25	111.00	163.00	229.25
	W_s (%)	0.260	0.389	0.534	0.693	0.865	1.048	1.243
	$\sigma_{r,\max}(\frac{kg}{cm^2})$	50.516	69.007	87.337	105.565	123.646	141.598	159.550
	CWO_{cr} (mm)	0.01562	0.02476	0.03432	0.04453	0.05515	0.06604	0.07734
GRKPM	T_{cr} (days)	10.25 [2.50]	22.75 [1.11]	42.75 [1.18]	72.00 [1.05]	111.50 [0.45]	163.50 [0.31]	229.25 [0.00]
	W_s (%)	0.263 [1.15]	0.391 [0.51]	0.537 [0.56]	0.696 [0.43]	0.867 [0.23]	1.050 [0.19]	1.243 [0.00]
	$\sigma_{r,\max}(\frac{kg}{cm^2})$	50.534 [0.04]	68.860 [0.21]	87.336 [0.00]	105.356 [0.20]	123.190 [0.37]	140.800 [0.56]	158.174 [0.86]
	CWO_{cr} (mm)	0.01600 [2.43]	0.02477 [0.00]	0.03488 [1.63]	0.04519 [1.48]	0.05568 [0.96]	0.06684 [1.21]	0.07828 [1.21]
$\beta = 0.10$								
Analytical	T_{cr} (days)	10.75	25.75	51.25	90.75	148.00	227.75	334.25
	W_s (%)	0.269	0.417	0.588	0.782	0.999	1.239	1.501
	$\sigma_{r,\max}(\frac{kg}{cm^2})$	50.517	69.007	87.335	105.563	123.190	141.595	159.550
	CWO_{cr} (mm)	0.01542	0.02462	0.03432	0.04450	0.05504	0.06599	0.07721
GRKPM	T_{cr} (days)	11.00 [2.32]	26.25 [1.94]	52.25 [1.95]	92.00 [1.38]	149.75 [1.18]	229.75 [0.88]	336.50 [0.67]
	W_s (%)	0.272 [1.11]	0.421 [0.95]	0.593 [0.85]	0.787 [0.64]	1.004 [0.50]	1.244 [0.40]	1.506 [0.33]
	$\sigma_{r,\max}(\frac{kg}{cm^2})$	50.534 [0.03]	68.861 [0.21]	87.335 [0.00]	105.355 [0.2]	123.191 [0.00]	140.799 [0.56]	158.172 [0.86]
	CWO_{cr} (mm)	0.01581 [2.53]	0.02470 [0.32]	0.03485 [1.54]	0.04499 [0.00]	0.05558 [0.98]	0.06653 [0.82]	0.07776 [0.71]
$\beta = 0.20$								
Analytical	T_{cr} (days)	11.75	29.50	61.00	112.75	190.75	303.50	443.75
	W_s (%)	0.281	0.446	0.641	0.872	1.134	1.430	1.730
	$\sigma_{r,\max}(\frac{kg}{cm^2})$	50.520	69.005	87.334	105.563	123.644	141.594	159.548
	CWO_{cr} (mm)	0.01522	0.02449	0.03419	0.04448	0.05503	0.06595	0.07719
GRKPM	T_{cr} (days)	12.00 [2.13]	30.00 [1.69]	62.50 [2.46]	115.00 [2.00]	194.25 [1.83]	308.25 [1.57]	450.25 [1.46]
	W_s (%)	0.284 [1.1]	0.450 [0.90]	0.649 [1.24]	0.880 [0.92]	1.144 [0.88]	1.441 [0.77]	1.742 [0.69]
	$\sigma_{r,\max}(\frac{kg}{cm^2})$	50.535 [0.03]	68.861 [0.21]	87.335 [0.00]	105.354 [0.20]	123.190 [0.37]	140.798 [0.56]	158.172 [0.86]
	CWO_{cr} (mm)	0.01562 [2.63]	0.02456 [0.29]	0.03477 [1.76]	0.04498 [1.12]	0.05557 [0.98]	0.06649 [0.82]	0.07774 [0.71]
$\beta = 0.30$								
Analytical	T_{cr} (days)	12.75	33.25	71.75	137.00	239.00	390.50	605.75
	W_s (%)	0.293	0.473	0.695	0.961	1.269	1.622	2.020
	$\sigma_{r,\max}(\frac{kg}{cm^2})$	50.525	69.005	87.333	105.561	123.644	141.595	159.548
	CWO_{cr} (mm)	0.01504	0.02435	0.03428	0.04445	0.05502	0.06595	0.07718
GRKPM	T_{cr} (days)	13.25 [3.92]	34.25 [3.01]	73.75 [2.79]	140.50 [2.56]	244.50 [2.30]	398.75 [2.11]	617.50 [1.94]
	W_s (%)	0.299 [2.05]	0.480 [1.48]	0.705 [1.44]	0.973 [1.25]	1.283 [1.10]	1.639 [1.05]	2.040 [0.99]
	$\sigma_{r,\max}(\frac{kg}{cm^2})$	50.535 [0.02]	68.862 [0.21]	87.334 [0.00]	105.354 [0.20]	123.189 [0.37]	140.798 [0.56]	158.171 [0.86]
	CWO_{cr} (mm)	0.01540 [2.39]	0.02441 [0.25]	0.03474 [1.34]	0.04497 [1.17]	0.05555 [0.96]	0.06649 [0.82]	0.07771 [0.69]

results of the GRKPM and those of the analytical solution. It is understood that the values of T_{cr} and $\sigma_{r,\max}$ increase as the amount of R_{con}/R_{st} increases for various values of β. These results are in line with those of other researchers for the case of $\beta = 0$, [5,11,19]. For a constant value of β, the values of parameters W_s and CWO_{cr} increase as the amount of R_{con}/R_{st} increases. Moreover, for a constant value of R_{con}/R_{st}, the variation of β has no significant effect on the maximum value of the interface's radial stress.

To examine the convergence of the proposed numerical solution, the percentage relative errors pertinent to GRKPM solutions for T_{cr} and W_s are displayed in Fig. 6. The results have been presented for the designed specimen III with $\beta = 0.3$. The number of distributed particles inside both media, steel and concrete are also identical. As is seen the percentage relative errors associated with T_{cr} and W_s decrease with an increasing number of particles. The relative error of the predicted values of W_s and T_{cr} by GRKPM becomes lower than 0.5% as the total number of particles becomes greater than 34.

The time history plots of the radial and hoop stresses at the interface of rust and concrete, and the radius of the zone containing the crack front have been depicted in Figs. 7–9 for specimen III. Each plot presents the time history of the parameter for three values of R_{con}/R_{st}; 3, 4 and 5 and the specified value of parameter β. Fig. 7(a)–(b) present the time history of the interfacial radial stress for $\beta = 0.0$ and $\beta = 0.5$, respectively. It is clear that there is a good agreement between the results of the GRKPM and the analytical approach. The maximum relative error of the radial stress of the GRKPM for $R_{con}/R_{st} = 3$, 4 and 5 is 0.0054, 0.0100, and 0.0113 for the case of $\beta = 0.0$; and 0.0055, 0.0100, and 0.0148 for the case of $\beta = 0.5$, respectively. The time history of the interface hoop stress in the concrete medium has been presented for $\beta = 0.0$ and $\beta = 0.5$ in Fig. 8(a) and (b). For clarity of these figures, only two different values of R_{con}/R_{st} have been displayed. It is observed that the GRKPM solution is in good agreement with the analytical prediction. It is evident that the higher value of β requires a longer time for the hoop stress within the concrete to reach its critical tensile strength. Fig. 9(a)–(b) present the time history of crack front radius for the case of $\beta = 0.0$ and $\beta = 0.5$, respectively. It is obvious that there is a reasonably

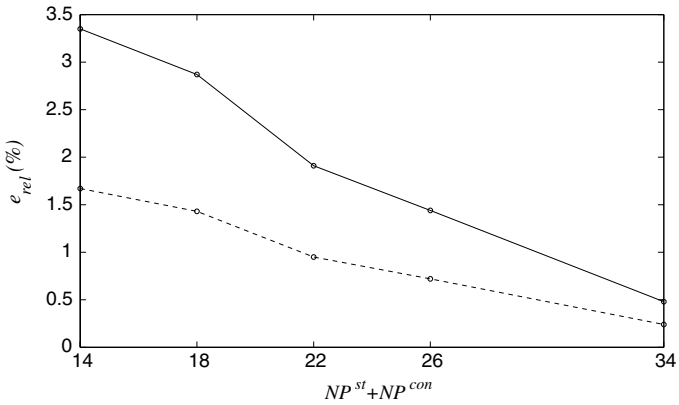

Fig. 6. The percentage relative error pertinent to GRKPM solutions for T_{cr} and W_s; — e_{rel} of T_{cr}, – – – e_{rel} of W_s.

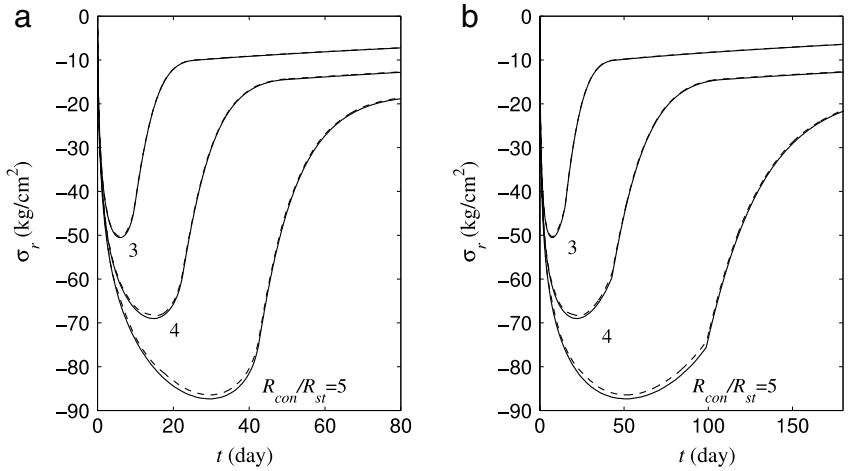

Fig. 7. Comparison of the predicted values for radial stress at the interface of rust and concrete via GRKPM and analytical approach for: (a) $\beta = 0.0$, and (b) $\beta = 0.5$; — Analytical approach, – – – GRKPM.

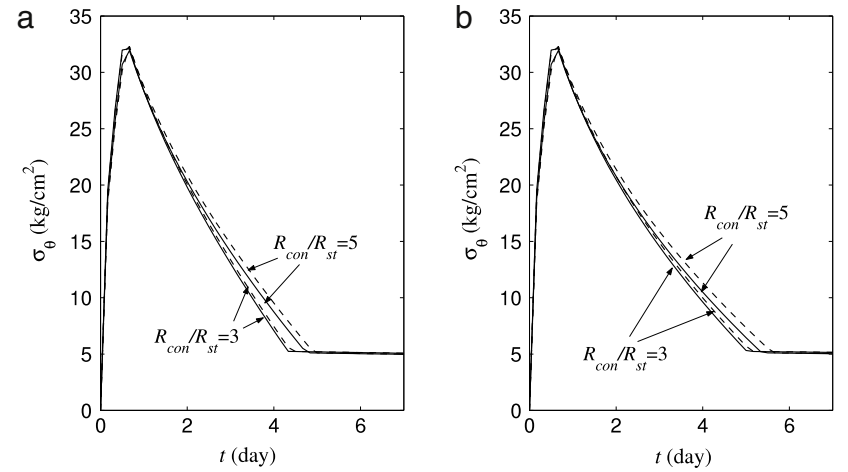

Fig. 8. Comparison of the predicted values for hoop stress at interface of rust and concrete in concrete medium via GRKPM and analytical approach for: (a) $\beta = 0.0$, and (b) $\beta = 0.5$; — Analytical approach, – – – GRKPM.

good agreement between the results of the two methods. It is also clear that with a good approximation, the time of crack initiation is independent of R_{con}/R_{st}.

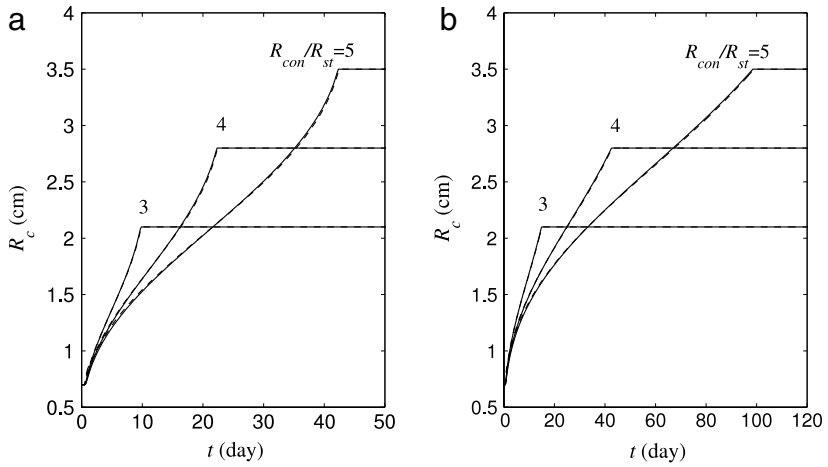

Fig. 9. Comparison of the predicted values for radius of smeared crack front via GRKPM and analytical approach for: (a) $\beta = 0.0$, and (b) $\beta = 0.5$; — Analytical approach, – – – GRKPM.

Table 4
Experimentally observed data for beam specimens by Rasheeduzzafar et al. [39].

Design specimen	D_{st} (cm)	C (cm)	f_c' (MPa)	i_{corr} $\left(\frac{\mu A}{cm^2}\right)$	W_s (%)	T_{cr} (h)
R_1	0.8	3.680	35.4	3000	2.75	60

Table 5
Experimentally observed data for slab specimens by Liu [33].

Design specimen	D_{st} (cm)	C (cm)	f_c' (MPa)	i_{corr} $\left(\frac{\mu A}{cm^2}\right)$
L_1	1.6	7.0	31.5	1.79
L_2	1.27	5.2	31.5	1.80

Table 6
Comparison of the time to cover cracking and amount of consumed rebar given by the experiment of Liu [33] for slab specimens with those computed by Bhargava et al. [10] and the present work.

Design specimen	Experimentally observed data of Liu [33]	Bhargava et al. [10] based on Liu model [33]		Bhargava et al. model [10]	Present study	
		$r_m = 0.523$	$r_m = 0.622$	$r_m = 0.613$	$r_m = 0.523$	$r_m = 0.622$
L_1 T_{cr} (yr)	3.54	3.34	4.49	5.06	3.76	5.45
L_2 T_{cr} (yr)	2.38	1.79	2.40	2.15	2.04	2.73

6.2. Comparison of the GRKPM results and the experimental data

In this part, the predicted results of the proposed model are compared with the experimental data and the results of other models for $C/R_{st} > 8$. The required data for each tested specimen including geometry, uniaxial compressive strength, and magnitude of applied corrosion current density to the specimen have been given in Tables 4 and 5. Moreover, the experimentally observed data, the predicted results of Bhargava et al. [10] based on the models of other researchers, and the results of the GRKPM are presented in Table 6. It is clear from Table 4 that the amount of corrosion current density subjected to the specimen is much more than the natural values that the specimens often experience in outdoor conditions (=3–10 (μA/cm^2) according to [38]). Therefore, it may be concluded that some of the corrosion products penetrate into the vacant spaces of the microcracks caused by rebar corrosion. Unfortunately, no useful data about the amount of rust diffused into the spaces of microcracks was reported in the experimental work of [39]. The value of β is chosen such that it leads to the best correspondence between the predicted and experimentally observed amount of consumed rebar for both of the specimens. This is done according to the least squares method. Throughout this paper, it is assumed that β

would be time independent, and microcracks would be visible at the concrete's surface when the dimension of crack width openings at the concrete's surface reaches 0.05 mm. A reasonably good agreement between the predicted results of W_s and the experimentally observed data is achieved for the case of $\beta = 0.20$. For this case, the proposed model predicts $W_s = 2.754(\%)$ and $T_{cr} = 16.8$ (h) based on $r_m = 0.622$. The model of Bhargava et al. [10] predicts $W_s = 2.719(\%)$ and $T_{cr} = 31.36$ (h) based on $r_m = 0.613$. It is obvious that there is a considerable difference between the predicted results of T_{cr} from both models with the reported data. More assessments show that the assumed value for $CWO_{surface}$ can highly affect on the predicted value of T_{cr}. For example, assuming $CWO_{surface} = 0.1$ (mm) would give $T_{cr} = 38.3$ (h) for $\beta = 0.20$. Nevertheless, the rust production model employed has been calibrated based on the test data of Liu [33] for outdoor conditions (i.e., $i_{corr} < 10\ (\mu A/cm^2)$). In contrast to the experimental tests of Liu [33], the present specimens were subjected to an accelerated corrosion test. This fact may also affect the values of the parameters associated with the model of rust production as well as the predicted values of T_{cr} and W_s.

Table 6 provides another comparison of the predicted values from the proposed model and other analytical models with the experimentally observed data of Liu [33] in terms of T_{cr}. For all of the specimens, the amount of the corrosion current density is lower than 5 ($\mu A/cm^2$). Therefore, it is assumed that no amount of corrosion products diffuses into the vacant spaces of microcracks, i.e., $\beta = 0$. For some of the specimens, the predicted time to cover cracking of the proposed model is somewhat greater than those of the experiment. The main reason is that for all of the specimens tested, most of the corrosion area was located on the upper part of the steel's surface (i.e., part of the steel's surface closer to the surface of the concrete slab) during the rebar's corrosion [33]. Therefore, the uniformity of the rebar's corrosion (second assumption as mentioned in Section 4) would not be satisfied exactly for these specimens. However, the results of the proposed model for $r_m = 0.523$ and 0.622 have been presented for further comparisons with the existing analytical models. It is obvious that the predicted values of the proposed model ($r_m = 0.523$) for T_{cr} are closer to the experimentally observed values for most of the specimens. Furthermore, this results are in line with those of Liu [33] for both specimens. The evolution of i_{corr} and the moisture content of the concrete specimens are the other important issues can affect the predicted results of T_{cr} and W_s, especially for long-term corrosion tests. In the next subsection, for designing a specimen, the effects of various parameters such as the mechanical properties of rust products and concrete on the substantial parameters of the rebar's corrosion, i.e., T_{cr}, W_s, $\sigma_{r,\max}$ and CWO_{cr} will be discussed in some detail.

6.3. Parametric study of the proposed model

The difference between the predicted values of the proposed model and the observed data from the outdoor (field) and indoor (laboratory) tests arises from various factors. The mechanical behavior of concrete and rust, the chemical composition of the corrosion products, and the parameter value of β are among the major issues affect on the response of RC structures subjected to the reinforcement's corrosion. In this part, the effects of the parameters associated with the mechanical properties of concrete and rust, on the interested parameters of rebar corrosion, i.e., T_{cr}, W_s, $\sigma_{r,\max}$ and CWO_{cr} are investigated for various values of β.

Consider a cylindrical reinforced concrete specimen with the following data: $D_{st} = 1.6$ (cm), $C = 2.7$ (cm) and $f'_c = 31.5\ (kg/cm^2)$ under uniform corrosion with $i_{corr} = 3.75\ (\mu A/cm^2)$. To analyze the effects of the above mentioned parameters, it is convenient to employ the following normalizations: $\overline{T}_{cr} = T_{cr}/T^*_{cr}$, $\overline{W}_s = W_s/W^*_s$, $\overline{E}_0 = E_0/E^*_0$, $\overline{f}_{ct,res} = f_{ct,res}/f^*_{ct,res}$, $\overline{f}_{ct} = f_{ct}/f^*_{ct}$, $\overline{\sigma}_{r,\max} = \sigma_{r,\max}/f_{ct}$ and $\overline{CWO}_{cr} = CWO_{cr}/CWO^*_{cr}$ wherein the parameters T^*_{cr}, W^*_s and CWO^*_{cr} are the predicted values of the specimen for $E^*_0 = 15\,100\sqrt{f'_c}$, $f^*_{ct} = 1.725\sqrt{f'_c}$, $f^*_{ct,res} = 0.15f^*_{ct}$. Fig. 10(a)–(d) present the normalized time to surface cracking ($\overline{T}_{cr}$) and the normalized amount of consumed rebar ($\overline{W}_s$) as a function of the normalized parameters related to the mechanical behavior of concrete such as $\nu_{r\theta}$, E_0, f_{ct}, and $f_{ct,res}$, respectively. Fig. 11(a)–(d) present $\overline{T}_{cr}$ and $\overline{W}_s$ as a function of r_m, α, K_{corr} and n_{corr}, respectively. As is seen in Figs. 10 and 11, for all of the values of the parameters considered herein, $\overline{T}_{cr}$ and $\overline{W}_s$ increase with β. The general trends of $\overline{T}_{cr}$ as a function of $\overline{E}_0$, $\overline{f}_{ct}$, $\overline{f}_{ct,res}$ and r_m are in line with the work of other researchers [10,11] for the special case of $\beta = 0$. A brief comparison of Figs. 10 and 11 reveals that the parameters r_m, α, E_0, $\overline{f}_{ct}$ and n_{corr} have more influence on the predicted values of $\overline{T}_{cr}$ and $\overline{W}_s$ than the others.

For different values of β, Fig. 12(a)–(d) present the normalized parameters of crack width openings at the time of surface cracking, $\overline{CWO}_{cr}$ and the maximum value of radial stress at rust–concrete interface, $\overline{\sigma}_{r,\max}$ as a function of $\nu_{r\theta}$, $\overline{E}_0$, $\overline{f}_{ct}$, and $\overline{f}_{ct,res}$. Fig. 12(a) shows that an increasing Poisson's ratio leads to a slight increase and decrease in the predicted values of $\overline{CWO}_{cr}$ and $\overline{\sigma}_{r,\max}$, respectively. Fig. 12(b) indicates that $\overline{CWO}_{cr}$ decreases as E_0 increases, whereas $\overline{\sigma}_{r,\max}$ increases with E_0. Fig. 12(c)–(d) show that an increase in tensile strength and residual tensile strength would result in the increase of the predicted values of $\overline{CWO}_{cr}$ and $\overline{\sigma}_{r,\max}$. A brief comparison of the slope of the depicted plots in Fig. 12(a)–(d) reveals that the variation of the parameters E_0 and f_{ct} have more effect on the variation of $\overline{CWO}_{cr}$ and $\overline{\sigma}_{r,\max}$ with respect to the other factors. Fig. 13(a)–(b) illustrate $\overline{CWO}_{cr}$ and $\overline{\sigma}_{r,\max}$ as a function of the parameters associated with rust properties, i.e., r_m, α, K_{corr}, and n_{corr} for various values of β. It is clear that for all of these parameters, the value of β has a very trivial effect on the predicted values of $\overline{CWO}_{cr}$ and $\overline{\sigma}_{r,\max}$. Similarly, for a constant β, variation of the mentioned parameters of the rust properties has a very slight effect on the variation of $\overline{CWO}_{cr}$ and $\overline{\sigma}_{r,\max}$. Moreover, the comparison of the demonstrated results in Fig. 12 with those shown in Fig. 13, reveals that the effects of the parameters associated with the mechanical behavior of concrete on the predicted values of $\overline{CWO}_{cr}$ and $\overline{\sigma}_{r,\max}$, are more significant than those related to the rust properties.

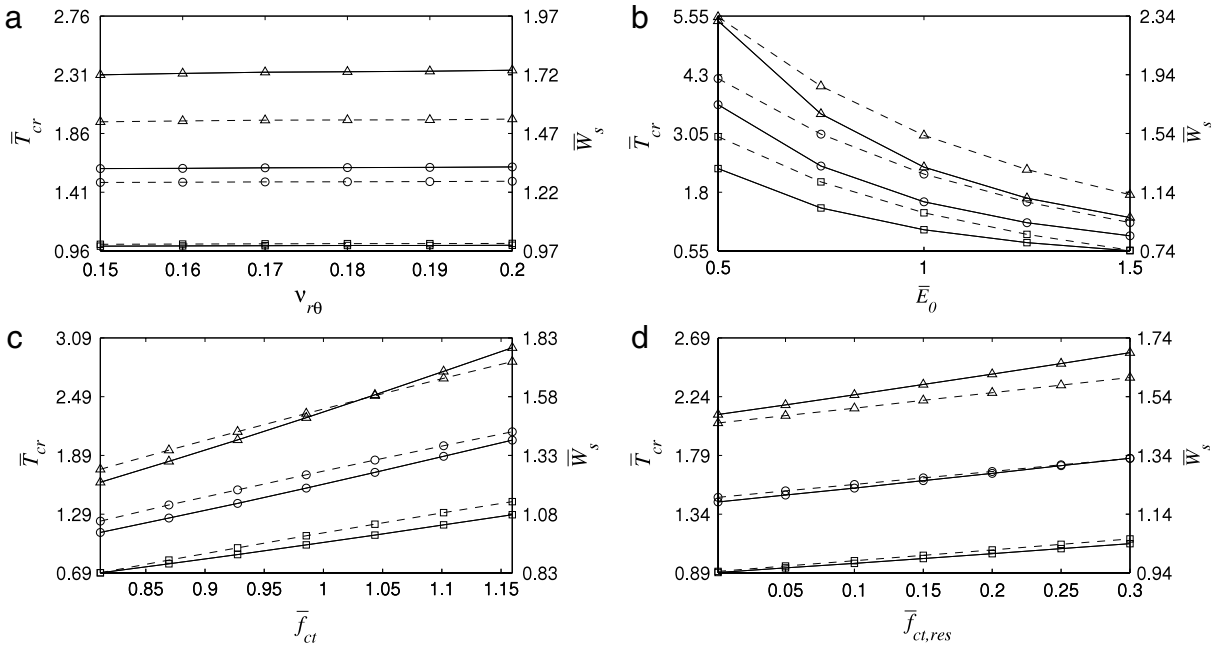

Fig. 10. Normalized time to concrete cover cracking ($\overline{T}_{cr}$) and normalized amount of consumed rebar ($\overline{W}_s$) as a function of: (a) $\nu_{r\theta}$, (b) $\overline{E}_0$, (c) $\overline{f}_{ct}$, and (d) $\overline{f}_{ct,res}$ for various values of β ($\square$ $\beta = 0.00$, $\circ$ $\beta = 0.25$, $\Delta\beta = 0.50$; — plot of $\overline{T}_{cr}$, - - - plot of $\overline{W}_s$).

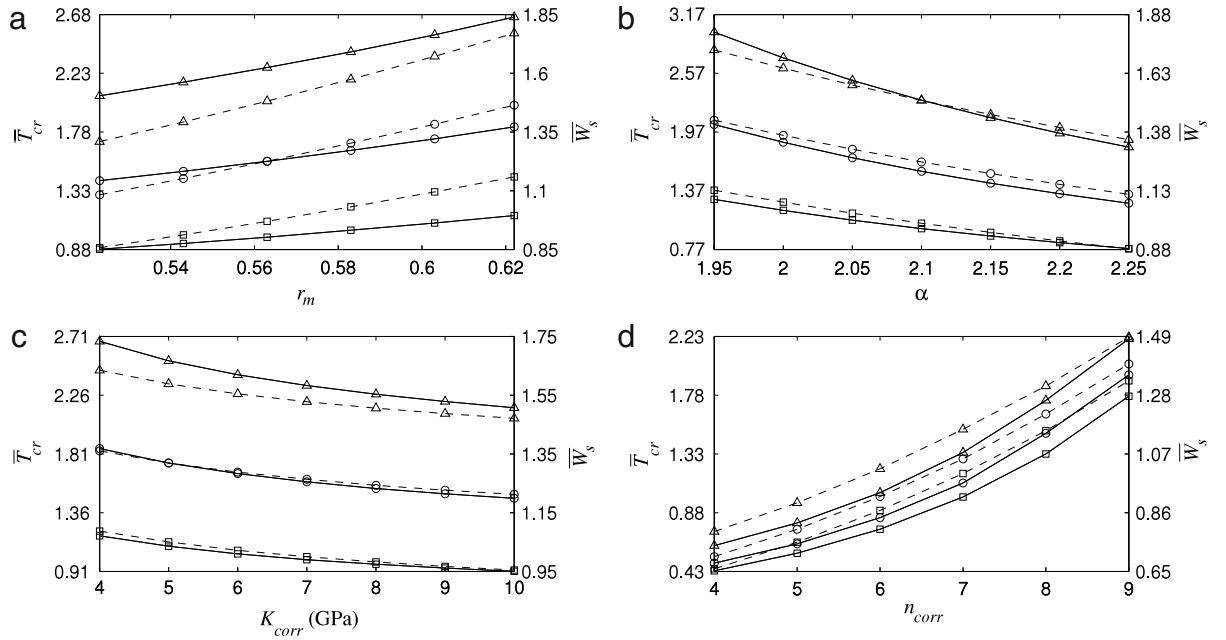

Fig. 11. Normalized time to concrete cover cracking ($\overline{T}_{cr}$) and normalized amount of consumed rebar ($\overline{W}_s$) as a function of: (a) r_m, (b) α, (c) K_{corr}, and (d) n_{corr} for various values of β ($\square$ $\beta = 0.00$, $\circ$ $\beta = 0.25$, $\Delta\beta = 0.50$; — plot of $\overline{T}_{cr}$, - - - plot of $\overline{W}_s$).

7. Conclusions

A nonlinear mathematical model is developed to determine the displacement and stress fields in RC structures due to rebar corrosion. The mechanical behavior of steel, rust and concrete is assumed to be linear isotropic, power law stress–strain relation and nonlinear anisotropic with postcracking softening, respectively. Presuming the radial strain of a thin film of rust as a nonlinear function of radial stress at the rebar–concrete interface and allowing penetration of corrosion products into the vacant spaces of microcracks as a nonlinear function of crack width openings yield to nonlinearity of the boundary

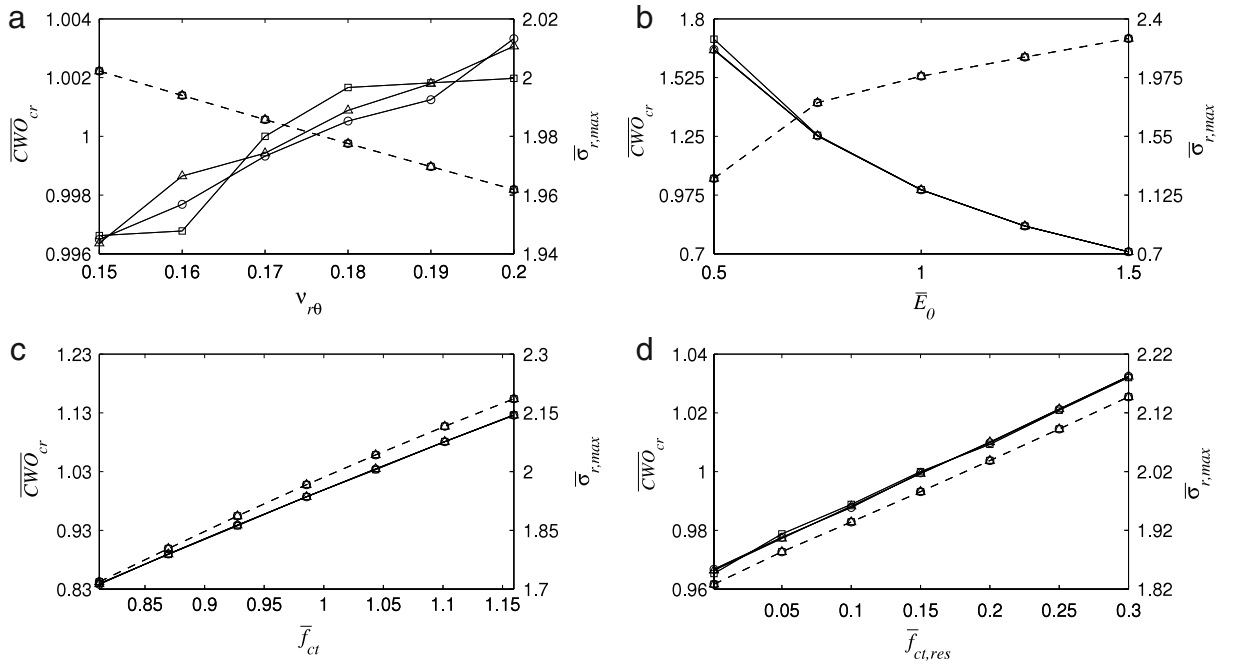

Fig. 12. Normalized crack width opening ($\overline{CWO}_{cr}$) and normalized maximum value of radial stress at the rust–concrete interface ($\overline{\sigma}_{r,\max}$) as a function of: (a) $\nu_{r\theta}$, (b) $\overline{E}_0$, (c) $\overline{f}_{ct}$, and (d) $\overline{f}_{ct,res}$ for various values of β (□ $\beta = 0.00$, ∘ $\beta = 0.25$, $\Delta\beta = 0.50$; — plot of $\overline{CWO}_{cr}$, - - - plot of $\overline{\sigma}_{r,\max}$).

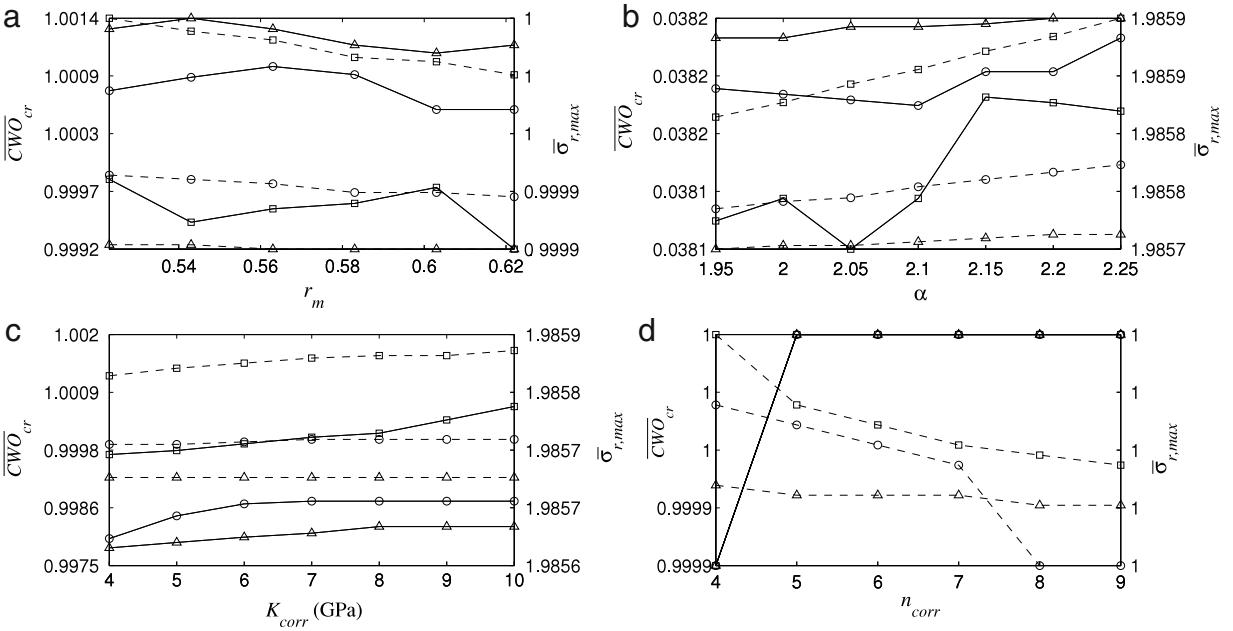

Fig. 13. Normalized crack width opening ($\overline{CWO}_{cr}$) and normalized maximum value of radial stress at the rust–concrete interface ($\overline{\sigma}_{r,\max}$) as a function of: (a) r_m, (b) α, (c) K_{corr}, and (d) n_{corr} for various values of β; (□ $\beta = 0.00$, ∘ $\beta = 0.25$, $\Delta\beta = 0.50$; — plot of $\overline{CWO}_{cr}$, - - - plot of $\overline{\sigma}_{r,\max}$).

condition of the governing equation for steel–rust–concrete composite media. The mathematical model has been analyzed both numerically and analytically with good correspondence; the minimum and maximum discrepancies in the results are about 0.1% and 3%, correspondingly. The predicted values of the effected parameters have been verified with those of experimentally observed data. The available experimental tests [33,39] do not provide sufficient data about the chemical composition and physical properties of corrosion products. Hence, the approach of Liu [33] is adopted for choosing a range of values for r_m, which is an indication of the chemical composition of rust. Moreover, there is no observed data about the amount of corrosion products which penetrate into the vacant spaces of microcracks during the corrosion processes.

Therefore, the volume fraction of the microcracks filled with the rust (β) is estimated based on the best correspondence between the predicted and experimental data for the amount of consumed rebar. It is observed that for low values of corrosion current density ($i_{corr} < 10\ \mu A/cm^2$), which is often produced by rebar corrosion in normal climate conditions, choosing $\beta \approx 0$ leads to a fairly good agreement between the model's predicted values and those of experiments. The parametric study and sensitivity analysis of the model have been performed in terms of various mechanical parameters of the concrete and rust. The present study shows that the parameter β has a vital effect on the predicted values of time to cover cracking and amount of consumed rebar. However, the values of maximum radial stress and crack width openings at the rust–concrete interface slightly decrease as β increases. To the best knowledge of the authors, the amount of corrosion products diffused into the vacant spaces of the microcracks is an open problem which requires further investigation.

Appendix

The elements of matrix $\mathbf{K}$ are as,

$$
\begin{array}{lll}
\mathbf{K}_{11} = -R_{cb}, & \mathbf{K}_{12} = \mathcal{P}_1(R_r), & \mathbf{K}_{13} = \mathcal{Q}_1(R_r), \\
\mathbf{K}_{21} = D^{st}_{rr} + D^{st}_{r\theta}, & \mathbf{K}_{22} = -\mathcal{R}_1(R_r), & \mathbf{K}_{23} = -\mathcal{S}_1(R_r), \\
\vdots & \vdots & \\
\mathbf{K}_{(2i+1)(2i)} = \mathcal{P}_i(r_i), & \mathbf{K}_{(2i+1)(2i+1)} = \mathcal{Q}_i(r_i), & \\
\mathbf{K}_{(2i+1)(2i+2)} = -\mathcal{P}_{i+1}(r_i), & \mathbf{K}_{(2i+1)(2i+3)} = -\mathcal{Q}_{i+1}(r_i), & \\
\mathbf{K}_{(2i+2)(2i)} = \mathcal{R}_i(r_i), & \mathbf{K}_{(2i+2)(2i+1)} = \mathcal{S}_i(r_i), & \\
\mathbf{K}_{(2i+2)(2i+2)} = -\mathcal{R}_{i+1}(r_i), & \mathbf{K}_{(2i+2)(2i+3)} = -\mathcal{S}_{i+1}(r_i), & \\
\vdots & \vdots & \\
\mathbf{K}_{(2N+1)(2N)} = \mathcal{R}_N(r_N), & \mathbf{K}_{(2N+1)(2N+1)} = \mathcal{S}_N(r_N). &
\end{array}
\tag{56}
$$

References

[1] Z.P. Bazant, Physical model for steel corrosion in concrete sea structures-theory, ASCE J. Struct. Div. 105 (1979) 1137–1153.
[2] K. Tutti, Corrosion of steel in concrete. Report No. 4 of Swedish Cement and Concrete Research Institute, Stockholm, Sweden, 1982.
[3] P. Schiessl, Corrosion of steel in concrete, RILEM Report of Technical Committee 60-CSC, 1988.
[4] H.J. Dagher, S. Kulendran, Finite element of corrosion damage in concrete structures, ACI Struct. J. 89 (1992) 699–708.
[5] F.J. Molina, C. Alonso, C. Andrade, Cover cracking as a function of rebar corrosion: part II-numerical model, Mater. Struct. 26 (1993) 532–548.
[6] C. Andrade, C. Alonso, F.J. Molina, Cover cracking as a function of rebar corrosion: part I-experimental test, Mater. Struct. 26 (1993) 453–464.
[7] K. Noghabai, Environmental effects on bond in reinforced concrete structures, in: Durability of Building Materials and Components, Proceedings of an International Conference, Stockholm, 1996, pp. 605–614.
[8] S. Morinaga, Prediction of Service Lives of Reinforced Concrete Buildings Based on Rate of Corrosion of Reinforcing Steel, Special report of the institute of Technology, Japan, Skimiza Corporation, 1989.
[9] Y. Liu, R.E. Weyers, Modeling the time-to-corrosion cracking in chloride contaminated reinforced concrete structures, ACI Mat. J. 95 (1998) 675–681.
[10] K. Bhargava, A.K. Ghosh, Y. Mori, S. Ramanujam, Model for cover cracking due to rebar corrosion in RC structures, Eng. Struct. 28 (2006) 1093–1109.
[11] S.J. Pantazopoulou, K.D. Papoulia, Modeling cover-cracking due to reinforcement corrosion in RC structures, ASCE J. Eng. Mech. 128 (2001) 342–351.
[12] K. Kiani, Study of reinforcement corrosion in RC structures via reproducing kernel particle method. M.Sc. Thesis. Tehran, Sharif University of Technology, 2002.
[13] K. Lundgren, Modeling the effect of corrosion on bond in reinforced concrete, Mag. Concr. Res. 54 (2002) 165–173.
[14] G.J. Al-Sulaimani, M. Kaleemullah, I.A. Basunbul, Rasheeduzzafar, Influence of corrosion and cracking on bond behaviour and strength of reinforced concrete members, ACI Struct. J. 87 (1990) 220–231.
[15] J.G. Cabrera, P. Ghoddoussi, The effect of reinforcement corrosion on the strength of the steel-concrete bond, in: Bond in Concrete, Proceedings of an International Conference, CEB, Riga, 1992.
[16] M. Ghandehari, M. Zulli, S.P. Shah, Influence of corrosion on bond degradation in reinforced concrete, in: Proceedings EM2000, Fourteenth Engineering Mechanics Conference, ASCE, Austin, Texas, USA, ASCE, 2000.
[17] K. Lundgren, Bond between ribbed bars and concrete: part 2. The effect of corrosion, Mag. Concr. Res. 57 (2005) 383–395.
[18] A. Ouglova, Y. Berthaud, M. Francois, F. Foct, Mechanical properties of an iron oxide formed by corrosion in reinforced concrete structures, Corros. Sci. 48 (2006) 3988–4000.
[19] K. Bhargava, A.K. Ghosh, Y. Mori, S. Ramanujam, Analytical model for time to cover cracking in RC structures due to rebar corrosion, Nucl. Eng. Des. 236 (2006) 1123–1139.
[20] K. Bhargava, A.K. Ghosh, Y. Mori, S. Ramanujam, Modeling of time to corrosion-induced cover cracking in reinforced concrete structures, Cem. Concr. Res. 35 (2005) 2203–2218.
[21] W.K. Liu, S. Jun, Y.F. Zhang, Reproducing kernel particle methods, Internat. J. Numer. Methods Fluids 20 (1995) 1081–1106.
[22] H.M. Shodja, A. Hashemian, A remedy to gradient type constraint dilemma encountered in RKPM, Adv. Eng. Softw. 38 (2007) 229–243.
[23] A. Hashemian, H.M. Shodja, Gradient reproducing kernel particle method, J. Mech. Mat. Struct. 3 (2008) 127–152.
[24] A. Hashemian, H.M. Shodja, A meshless approach for solution of Burgers' equation, J. Comput. Appl. Math. 220 (2008) 226–239.
[25] H.M. Shodja, A. Hashemian, A numerical solution of 2D Buckley–Leverett equation via gradient reproducing kernel particle method, Comput. Model. Eng. Sci. 32 (2008) 17–33.
[26] T. Belytschko, Y.Y. Lu, L. Gu, Crack propagation by element-free Galerkin methods, Eng. Fract. Mech. 51 (2) (1995) 295–315.
[27] T. Belytschko, Y.Y. Lu, L. Gu, M. Tabbara, Element-free Galerkin methods for static and dynamic fracture, Internat. J. Solids Structures 32 (17–18) (1995) 2547–2570.
[28] T. Rabczuk, T. Belytschko, Cracking particles: a simplified meshfree method for arbitrary evolving cracks, Internat. J. Numer. Methods Engrg. 61 (13) (2004) 2316–2343.
[29] T. Rabczuk, G. Zi, S. Bordas, H. Nguyen-Xuan, A geometrically non-linear three-dimensional cohesive crack method for reinforced concrete structures, Eng. Fract. Mech. 75 (16) (2008) 4740–4758.
[30] V.P. Nguyen, T. Rabczuk, S. Bordas, M. Duflot, Meshless methods: a review and computer implementation aspects, Math. Comput. Simulation 79 (3) (2008) 763–813.

[31] G.R. Liu, K.Y. Dai, T.T. Nguyen, A smoothed finite element method for mechanics problems, Comput. Mech. 39 (2007) 859–877.
[32] H. Nguyen-Xuan, S. Bordas, H. Nguyen-Dang, Smooth finite element methods: Convergence, accuracy and properties, Internat. J. Numer. Methods Engrg. 74 (2008) 75–208.
[33] Y. Liu, Modeling the time to corrosion cracking of the cover concrete in chloride contaminated reinforced concrete structures, Ph.D. Thesis, Blacksburg, Virginia Polytechnic Institute and State University, 1996.
[34] I. Peter-Lazar, B. Gerard, Mechanical behavior of corrosion products formed at the steel-concrete interface, testing and modeling, in: Proceedings EM2000, Fourteenth Engineering Mechanics Conference, Austin, Texas, USA, ASCE 2000.
[35] A.M. Kaynia, Structural Analysis of Reinforced Concrete Structures, Isfahan University of Technology Press, Isfahan, Iran, 1998.
[36] Comité Euro-International du Béton-Fédération International de la Précontrainte, (CEB-FIP) Design Code, London: Thomas Telford, 1990.
[37] Z.P. Bazant, B. Oh, Crack-bond theory for fracture of concrete, Mater. Struct. 16 (1983) 155–177.
[38] C. Alonso, C. Andrade, J. Rodriguez, J.M. Diez, Factors controlling cracking of concrete affected by reinforcement corrosion, Mater. Struct. 31 (1998) 435–441.
[39] S.S. Rasheeduzzafar, A.S. Al-Saadoun, Al-Gahtani, Corrosion cracking in relation to bar diameter, cover and concrete quality, ASCE J. Mater. Civ. Eng. 4 (1992) 327–343.